2016

Assembly and regulation of the DREAM complex

Jessica G. Felthousen
Virginia Commonwealth University, jfelthousen@vcu.edu

ASSEMBLY AND REGULATION OF THE DREAM COMPLEX

A thesis submitted in partial fulfillment of the requirements of the degree of Master of Science at Virginia Commonwealth University.

By

Jessica Felthousen
B. S., Marymount University, Arlington, VA

Thesis Director: Larisa Litovchick, M.D., Ph.D.
Assistant Professor
Division of Hematology/Oncology and Palliative Care
Department of Internal Medicine

Virginia Commonwealth University
Richmond, Virginia
April, 2016

ACKNOWLEDGMENTS

First, I would like to thank my advisor Dr. Larisa Litovchick, for giving me the opportunity to work in her laboratory. As a mentor, she has been a constant source of inspiration, motivation and support, who has patiently answered all my questions and kindly guided me through some tough decisions. Also, I would like to thank her for her numerous inputs throughout the compilation of this thesis. This work would not have been possible without her advice.

I thank my thesis committee members Dr. Jolene Windle and Dr. Andrew Larner for guiding me through this project with their knowledge, helpful advice, and generous suggestions. I especially thank Dr. Jolene Windle, for her support and advice during some challenging career decisions. Her kind words were truly inspiring.

I thank Dr. Seth Rubin for giving me the opportunity to collaborate on some of his projects. Also, I would like to thank him for his helpful suggestions and for providing some materials throughout my thesis project.

I would like to thank all members of the Litovchick lab for their constant support. I express my sincere gratitude to Dr. Siddharth Saini for being so patient in training me during my first laboratory rotation. I thank Dr. Vijay Menon for setting my medium out in the mornings on numerous occasions and helping me with troubleshooting my experiments. I thank Sophia

Gruszecki, for being such a wonderful individual that always prepared and made all available reagents and provided assistance whenever needed. I thank Varsha Ananthapadmanabhan for being a great friend and source of support while juggling coursework and lab work, and for helping me with experiments whenever needed.

I thank Dr. Steven Grossman and his lab members for their varied inputs on my project. I also thank them for letting me use their fluorescent microscope for expression analysis as well as acquiring images.

Lastly, I would like to thank my mother, Kathy Felthousen and fiancé, Daniel Rusbasan for being a constant source of motivation, strength, love and support throughout the ups and downs of my graduate career. Without their help this journey would have been extremely difficult.

TABLE OF CONTENTS

LIST OF FIGURES

LIST OF ABBREVIATIONS AND SYMBOLS

20q	Long arm of chromosome 20
ATCC	American type culture collection
BSA	Bovine serum albumin
C24	Cysteine 24
Caf1	chromatin assembly factor
CDK	Cyclin dependent kinases
ChIP	Chromatin immunoprecipitation
DAPI	4',6-diamidino-2-phenylindole
DMEM	Dulbecco's modified Eagle medium
DNA	Deoxyribonucleic Acid
DP	Dimerization partner
DREAM	DP, RB-like, E2F and MuvB
dREAM	*Drosophila* RBF, E2f2, and Mip
DS	Down syndrome
DYRK	Dual specificity tyrosine related kinase
E22A	Glutamic acid 22 to alanine
E26	Glutamic acid 26

EDTA	Ethylenediaminetetraacetic acid
EGF	Epidermal growth factor
EGFR	Epidermal growth factor receptor
FBS	Fetal bovine serum
FOXM1	Forkhead box M1
G0/G1	Quiescence
G1	Gap phase 1
G2	Gap phase 2
GFP	Green fluorescence protein
h	Hour
HPV	Human papillomavirus
HRP	Horseradish peroxidase
IP	Immunoprecipitation
ITC	Isothermal titration calorimetry
LT	Large T antigen
MDS	Myelodysplastic syndrome
MEF	Mouse embryonic fibroblasts
MMB	Myb-MuvB
M-phase	Mitotic phase
MTT	3-(4,5-Dimethylthiazol-2-yl)-2,5-Diphenyltetrazolium Bromide
MudPIT	Multidimensional Protein Identification Technology

Muv	Multi-vulva phenotype
MYBL	Myb-related protein
N/ C terminal	Amino/ carboxy terminal
PAGE	Polyacrylamide gel electrophoresis
PBS	Phosphate buffered saline
pMSCV	Murine stem cell virus expression system plasmid
RB	Retinoblastoma
RT	Room temperature
S20	Serine 20
S20C	Serine 20 to cysteine
S28	Serine 28
S28A	Serine 28 to alanine
SDS	Sodium dodecyl sulfate
S-phase	Synthesis phase
SV40	Simian virus 40
synMuv	Synthetic multi-vulva phenotype
T401A	Threonine 401 to alanine
T417A	Threonine 417 to alanine
TAP	Tandem affinity purification
TBS	Tris buffered saline
Tris- HCl	Tris hydrochloride
TTAA	T401A/T417A double mutant

VCM	Virus condition medium
WT	Wild type
β-ME	β-Mercaptoethanol

ABSTRACT

ASSEMBLY AND REGULATION OF THE DREAM COMPLEX

By, Jessica Grace Felthousen B. S., Marymount University, Arlington, VA

A thesis submitted in partial fulfillment of the requirements of the degree of Master of Science at Virginia Commonwealth University.

Virginia Commonwealth University, 2016

Thesis Director: Larisa Litovchick, M.D., Ph.D.
Assistant Professor
Division of Hematology/Oncology and Palliative Care
Department of Internal Medicine

The DREAM complex assembles during G0/G1 when RB-like protein p130 recruits E2F4, DP1, and a core complex of five MuvB proteins to repress genes involved in cell cycle progression. In

S-phase, the MuvB core dissociates from p130 and binds to BMYB transcription factor. Binding of the MuvB core to p130 requires phosphorylation of its subunit LIN52 at S28 residue by DYRK1A protein kinase. However, little is known about how the MuvB core interacts with p130 to form the DREAM complex, and how these interactions are manipulated throughout the cell cycle. In collaboration with Dr. Seth Rubin, we characterized the structural basis for DREAM assembly, and found that the LxSxExL sequence in LIN52 directly interacts with the LxCxE binding cleft within the pocket domain of p130. Furthermore, immunoprecipitation and proliferation assays revealed that mutating the LIN52 LxSxExL sequence to mimic the canonical LxCxE motif found in viral oncoproteins reduces cellular proliferation and stabilizes the DREAM complex in the presence of viral proteins. We addressed how the DREAM complex is disassembled upon cell cycle entry and found that CDK phosphorylation of p130 inactivates the DREAM complex by displacing p130 from the MuvB core. Under certain conditions, we found that BMYB and p130 simultaneously bind the MuvB core, while overexpression of BMYB disrupts DREAM assembly. Together, our study provides insight into the structural mechanisms of DREAM assembly and function, which can help identify novel approaches to halt tumor cell proliferation or dormancy.

CHAPTER 1: INTRODUCTION

1.1. The cell cycle

The cell cycle is an important process involved in cell growth and proliferation, development, deoxyribonucleic acid (DNA) damage repair, differentiation, and tumor development. The cell cycle encompasses G1, synthesis (S) phase, G2 and mitotic (M) phase (Figure 1) (reviewed in Cobrinik, 2005). The G1 and G2 phases of the cell cycle represent the "gaps" that occur between DNA synthesis and mitosis, where the DNA content shifts from 2N to 4N. During early G1, a decision is made to either continue another round of cell division or enter a state of dormancy known as G0 (reviewed in Malumbres & Barbacid, 2001; Schafer, 1998). In late G1, cells pass through the restriction point and prepare for S phase by transcribing genes needed for DNA synthesis (reviewed in DeGregori, 2002). Following the completion of S phase, the G2 phase is the second "gap" in which cells prepare for M phase by repairing any DNA damage and transcribing genes needed for mitosis (reviewed in Schafer, 1998).

1.2. Cell cycle exit

The decision to not continue another round of cell division and enter quiescence (G0/G1) is a critical step for tumor suppression and differentiation (reviewed in Malumbres & Barbacid, 2001). In response to certain stimuli, such as differentiation signals, nutrient starvation, contact inhibition, loss of adhesion and genotoxic stress, normal cells stop dividing and enter a quiescent state. Cancer cells acquire the ability to inactivate the pathways that control G0/G1 arrest

resulting in increased proliferation and tumor formation (reviewed in Malumbres & Barbacid, 2001). Furthermore, tumor cells utilize quiescence to escape therapeutic treatments that target dividing cells (reviewed in Aguirre-Ghiso, 2007). Therefore, identification and characterization of the molecular mechanisms that govern entry into quiescence are critical for designing therapeutic strategies to target tumor cell proliferation and cancer dormancy.

1.3. E2F family, pocket proteins and cell cycle control

In human cells, the G1 to S phase transition depends on the E2F family of transcription factors and their binding partners. The E2F family consists of eight E2F proteins, E2F1 to E2F8, and three heterodimeric partners, DP1, DP2 and DP3 (reviewed in DeGregori, 2002; Blais & Dynlacht, 2004; Lammens et al, 2009). The E2F proteins are split into two categories: transcriptional activators (E2F1, E2F2, and E2F3A) and repressors (E2F3B, E2F4, E2F5, E2F6, E2F7, and E2F8) (Figure 2B) (reviewed in Bertoli et al., 2013; Lammens et al, 2009). E2F proteins 1-6 (but not 7 or 8) have a conserved dimerization domain that is required to bind to DP proteins that enhance the ability of E2Fs to properly bind and regulate transcription of target genes (reviewed in DeGregori, 2002; Blais & Dynlacht, 2004; Lammens et al, 2009). In addition, most E2F proteins except for E2F6, E2F7, and E2F8 have a pocket protein domain, where pocket proteins known as the retinoblastoma (RB) family can bind and regulate E2F transcription factor activity (reviewed in Bertoli et al., 2013; Lammens et al, 2009).

The RB family of tumor suppressors consists of *RB1*, *RBL1* and *RBL2*, which serve both redundant and unique functions in the cell cycle (reviewed in Classon & Harlow, 2002). The respective protein products of these genes, pRb, p107, and p130, contain a highly conserved pocket domain that includes an E2F binding domain and an LxCxE binding cleft that binds proteins containing an LxCxE sequence (Figure 2A) (reviewed in Dick & Rubin, 2013). During early G1, activator E2F proteins are bound and inhibited by hypophosphorylated pRb, whereas E2F4 and E2F5 bind hypophosphorylated p130 and p107 to repress transcription (Figure 2B) (reviewed in Bertoli, 2013). In late G1, pocket proteins are hyperphosphorylated by cyclin dependent kinases (CDK) 4/6 and cyclin D complexes resulting in release of E2F proteins, followed by E2F-dependent transcription and cell cycle progression (Figure 1) (reviewed in Cobrinik, 2005). Interestingly, mouse genetic studies revealed that the RB family proteins have overlapping biological roles in controlling entry into quiescence. The RB-like proteins p107 and p130 can compensate one another in development, while RB plays a unique role in development. (Hurford et al, 1997; Dannenberg et al, 2004).

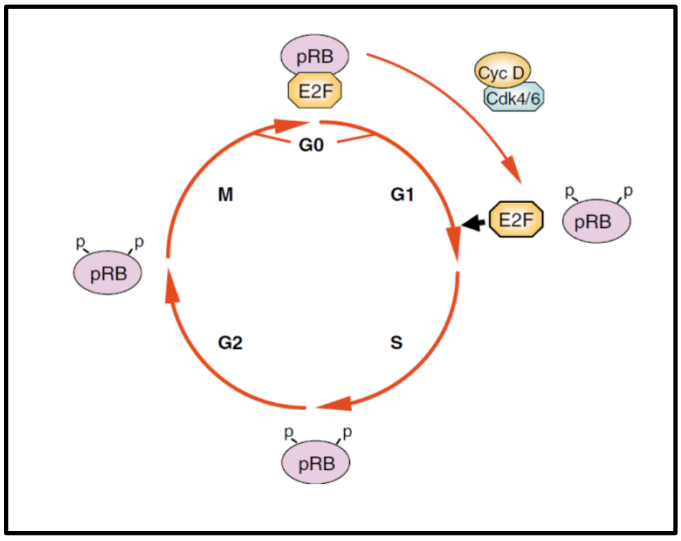

Figure 1. A schematic drawing of the G1 to S phase transition.
E2F is released following hyperphosphorylation of pRb by the CDK4/6-cyclin D complex. (Adopted from Cobrinik, 2005)

Despite the similarities between pocket proteins, there are significant differences between the RB family proteins. For example, p107 is only expressed in proliferating cells, whereas p130 is upregulated in quiescent cells (Hurford et al, 1997; Litovchick et al, 2007). RB and p107 undergo cell cycle dependent phosphorylation in mid-G1 to S phase, whereas p130 is phosphorylated in G0 and early G1 (Canhoto et al., 2000). Furthermore, p130 has additional modifications within its pocket domain that are functionally important for interacting with E2Fs in quiescent cells (Figure 2A) (reviewed in Classon & Harlow, 2002). Therefore, p130 appears to be uniquely involved in regulating and maintaining G0/G1.

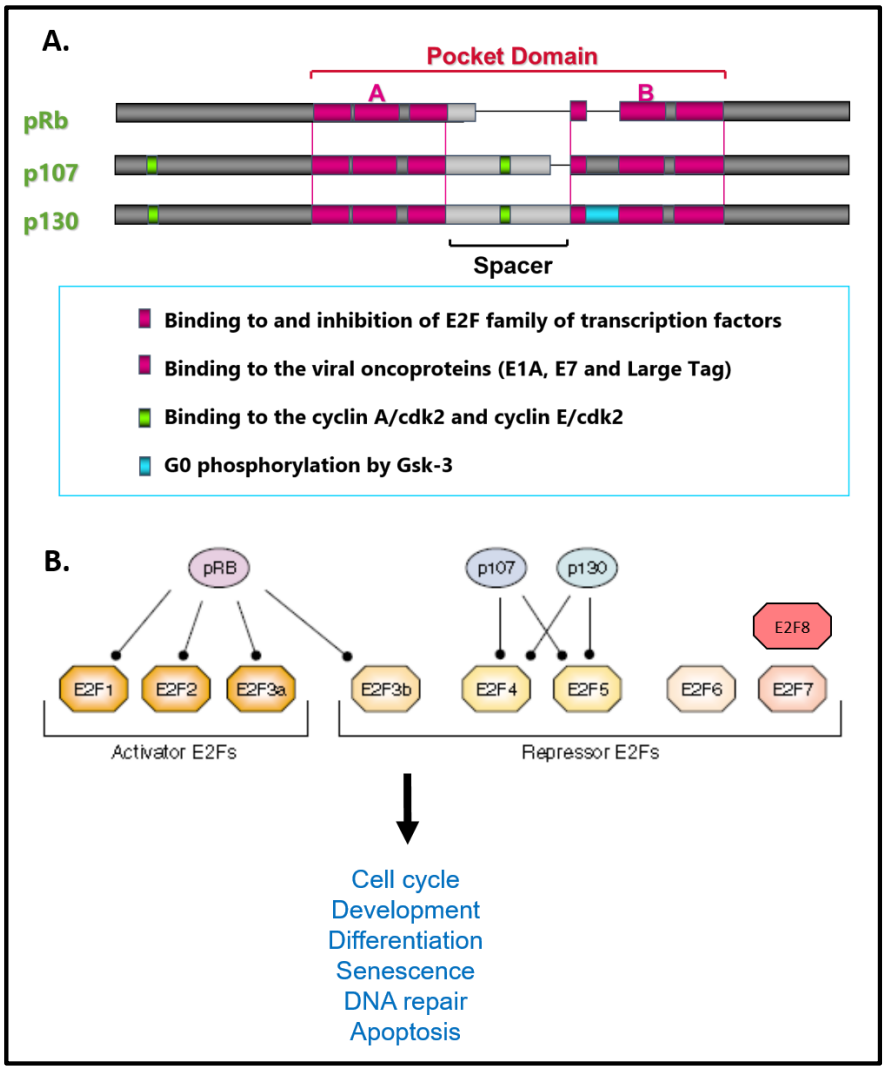

Figure 2. A schematic of the Retinoblastoma family structure and function.
(A) Each retinoblastoma (RB) family member has a highly conserved pocket domain that includes an E2F binding site and an LxCxE binding cleft (L. Litovchick, with permission). (B) The RB family proteins bind and regulate E2F transcription factor activity (Adapted from Cobrinik, 2005).

1.4. Identification of the conserved DREAM and MMB complexes

Several genetic studies involving *Caenorhabditis elegans* and *Drosophila melanogaster* contributed to the identification of evolutionally conserved cell cycle regulatory complexes, known as the DP, RB-like, E2F and MuvB (DREAM) and the Myb-MuvB (MMB) complexes. Previous studies in *C. elegans*, identified a set of genes known as Vul genes that control vulva development and encode homologues of epidermal growth factor (EGF), EGF receptor (EGFR)

and RAS (Aroian et al, 1990; Beital et al, 1990; Han & Sternberg, 1990). During vulva development, LIN-3, an EGF-like ligand signals to surrounding cells to activate a RAS signaling cascade needed for acquired vulval fate. Increased activation of Vul genes leads to a multi-vulva phenotype (Muv), which could be also seen upon the loss-of-function mutations in certain genes that oppose the EGF-EGFR-RAS signaling cascade required for normal vulva development (Ferguson et al, 1989). Since the Muv phenotype requires inactivation of two such genes simultaneously, they are termed the synthetic multi-vulva (synMuv) genes. Based on their genetic interaction with each other, the synMuv genes are grouped into three classes, A, B, and C (reviewed in Fay & Han, 2000). Importantly, several MuvB genes that antagonize RAS signaling in *C. elegans* encode homologues of genes in the RB-E2F pathway (Figure 3) (reviewed in Fay & Han, 2000).

Previous studies in *D. melanogaster* identified a complex that contains the Myb transcription factor and four Myb-interacting proteins homologous to the *C. elegans* MuvB genes: Mip120, Mip40, and chromatin assembly factor 1 (Caf1) (Figure 3). Given that the Mips have strong homology to the *C. elegans* synMuvB genes, the complex was named MMB (Beall et al, 2002). Another study focused on identifying proteins that are bound to the fly RB homologues RB-family protein 1 (Rbf1) and Rbf2, as well as E2f. Using *D. melanogaster* embryo extracts, a complex was purified containing Rbf1, Rbf2, Dp, E2f2, Myb and several homologues of the synMuvB genes, including Mip130, Mip120, Mip 40 and Caf1, and it was named the *Drosophila* RBF, E2f2 and Mip (dREAM) complex (Figure 3) (Korenjak et al, 2004). Therefore, in *D. melanogaster*, the MMB and dREAM complexes both contain Myb, and were found to function together as one transcriptional activator and repressor complex (Georlette, 2007; Lewis, 2004).

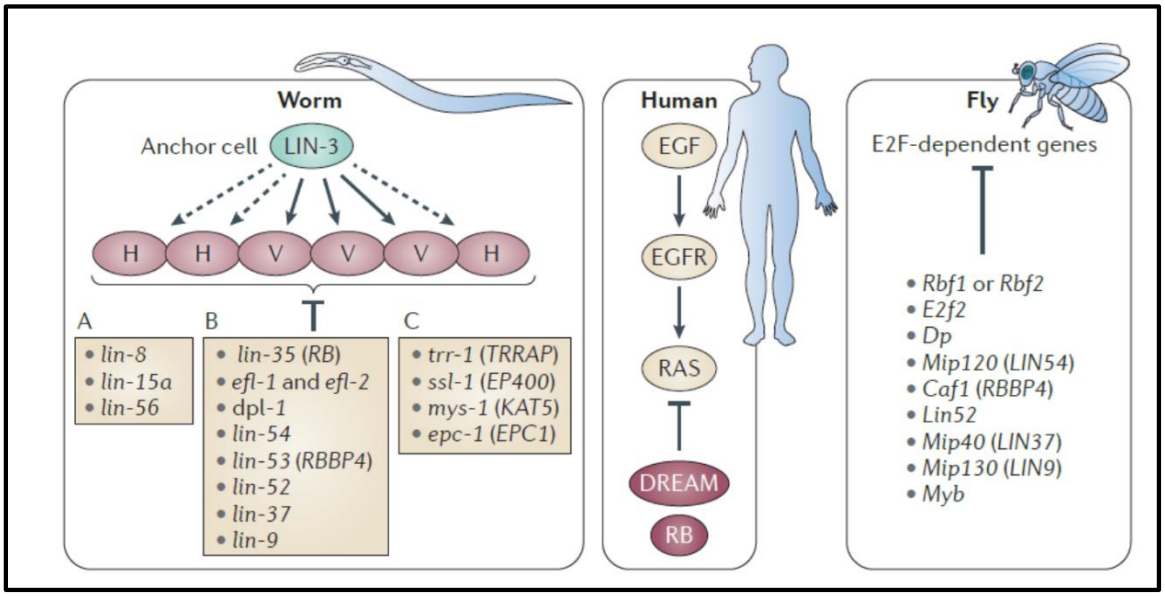

Figure 3. The Muv genes and their homologues.
In *C. elegans*, high levels of LIN-3 are required to overcome the repressive effects of the synthetic multi-vulval (synMuv) class of genes on RAS signaling. The synMuv genes are subclassed into A, B, and C. In humans, RB and the DREAM complex independently represses RAS signaling. In *D. melanogaster*, RB-E2F homologues, Myb, and the synMuvB genes are required to repress E2F target genes. Mammalian homologues are shown in brackets (Adopted from Sadasivam and DeCaprio, 2013).

In mammalian cells, immunoprecipitation of RB-like protein p130 followed by multidimensional protein identification technology (MudPIT) proteomic analysis identified a multiprotein complex that consisted of DP1, RB-like protein p130 or p107, E2F4 or E2F5, and five MuvB proteins (LIN9, LIN37, LIN52, LIN53/RBBP4, and LIN54), known as the DREAM complex (Figure 3 & 4) (Florens & Washburn, 2006; Litovchick et al, 2007). Unlike *D. melanogaster*, the mammalian DREAM complex does not contain a MYB family protein. Furthermore, the DNA binding factor BMYB co-precipitated the five MuvB proteins (MuvB core) but not p130, p107, E2F4 or DP1 (Pilkinton et al, 2007; Litovchick et al, 2007). As a result,

the MuvB core creates two distinct complexes by binding to p130 or p107 to form the DREAM complex or to BMYB to form the MMB complex (Figure 4).

1.5. Mammalian DREAM/MMB complexes assembly and regulation

Genome-wide chromatin immunoprecipitation (ChIP) studies identified significant overlap of binding enrichment for p130, E2F4, and MuvB proteins LIN9 and LIN54 in G0-arrested cells. Location analysis revealed that these overlapping binding sites are positioned close to the transcription start sites of cell cycle dependent genes (Litovchick et al, 2007). Furthermore, knockdown of the DREAM components led to an increase in cell cycle-dependent gene expression and cell cycle progression (Litovchick et al, 2007). As a result, p130, E2F4, and the MuvB core bind together as the DREAM complex to maintain quiescence and repress genes involved in cell cycle progression (Figure 4).

To identify the mechanism of DREAM complex assembly, proteomic analysis was used to detect novel phosphorylation sites of the DREAM components. It was found that serine 28 (S28) in LIN52 was present in its phosphorylated form when coimmunoprecipitated with p130 (Litovchick et al, 2011). In cell synchronization experiments followed by western blot analysis, phosphorylated LIN52 was enriched in quiescent cells when compared to cells in G1, S, and G2. Furthermore, when LIN52-S28 was mutated to an alanine (LIN52-S28A), binding between LIN52 and p130 was completely abolished (Litovchick et al, 2011). Together, these results demonstrate that phosphorylation of LIN52 at S28 is required for DREAM assembly during G0 (Figure 4).

Given that a LIN52-S28 phosphorylation event is required for DREAM assembly, MudPIT analysis was performed to identify the kinase responsible for this phosphorylation. According to the proteomic data, Dual-specificity tyrosine-(Y)-phosphorylation Regulated Kinase 1A

(DYRK1A) was identified in LIN52 immunoprecipitations (Litovchick et al, 2011). The DYRK family of kinases catalyzes the phosphorylation of serine/threonine residues on protein substrates, and are involved in cell cycle regulation or in controlling the transition from cell growth to differentiation (Becker et al, 1998). Mammals have five DYRK kinases of which DYRK1A is the most extensively characterized member. DYRK1A can recognize the conserved RX(X)(S/T)P consensus motif in its protein substrates including the residues surrounding the S28 phosphorylation site in LIN52 (Himpel et al, 2001; Becker et al, 1998; Litovchick et al, 2011). Importantly, an *in vitro* kinase assay revealed that recombinant DYRK1A directly phosphorylates S28 in LIN52. Furthermore, depleting cells of DYRK1A or inhibiting DYRK1A kinase activity by small molecule inhibitor harmine reduces the S28-LIN52 phosphorylation and abolishes the interaction between p130 and the MuvB core proteins, thus preventing cells from entering quiescence (Litovchick et al, 2011). Together, these results show that LIN52-S28 phosphorylation by DYRK1A is required to promote DREAM complex assembly and entry into quiescence.

Upon cell cycle entry, p130 dissociates from E2F4 and the MuvB core, resulting in activation of early cell cycle genes such as *MYBL2, CDC6* and *CDC2* (reviewed in Sadasivam et al, 2013). The protein product of *MYBL2,* BMYB, is a well characterized transcription factor that binds to the promoters of genes expressed in the G2/M phase, such as CDK1 and CCNB1 and activates their transcription (Zhu et al, 2004; Chen et al, 2013). According to immunoprecipitation data, the MuvB core associates with BMYB independent of p130 to form the Myb-MuvB (MMB) complex during S-phase (Figure 4) (Sadasivam et al, 2012; Pilkinton et al, 2007). Genome wide ChIP analysis revealed significant overlap between target promoters of BMYB and the MuvB core, where many of these binding sites were found in the promoters of

late cell cycle genes. Furthermore, knockdown studies showed that BMYB requires the presence of the MuvB core for binding to its target promoters, and vice versa (Sadasivam et al, 2012). Together, these results demonstrate that the MuvB core forms a complex with BMYB to bind target promoters in S-phase (Figure 4).

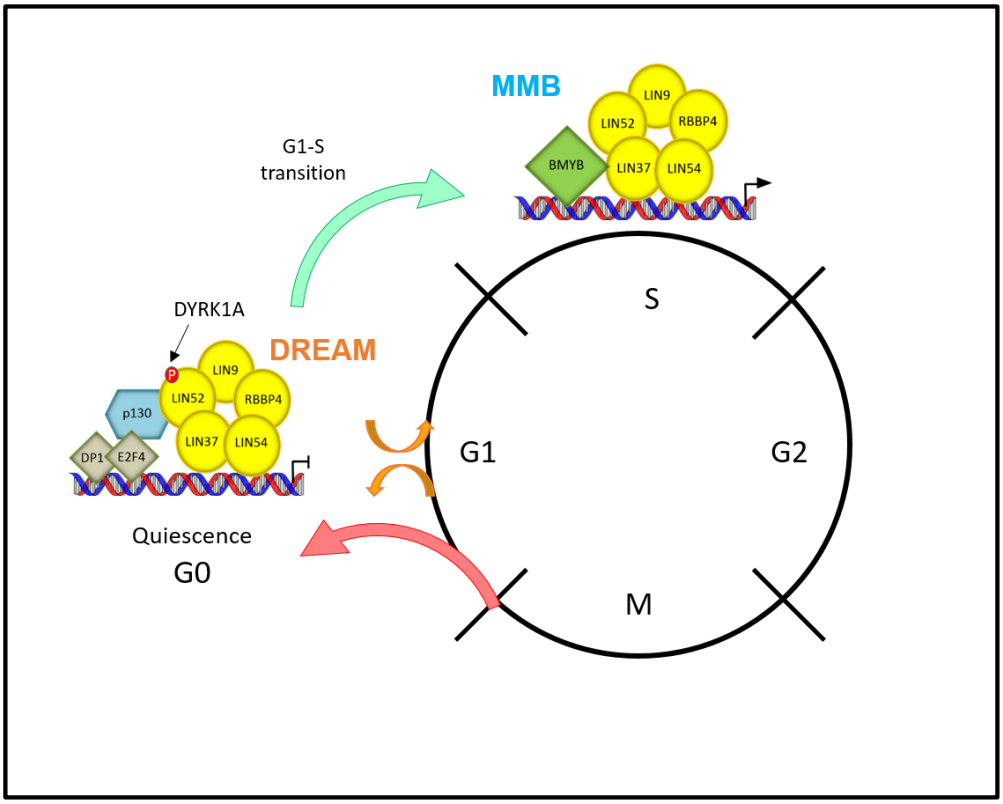

Figure 4. Differential cell cycle control by the DREAM and MMB complexes.
Both the DREAM and MMB complexes share the highly conserved MuvB core (yellow). To repress genes involved in cell cycle progression during G0/G1, the MuvB core associates with p130, E2F4, DP1 to form the DREAM complex. DYRK1A promotes DREAM assembly by phosphorylating the MuvB core subunit LIN52 at serine 28 (S28) resulting in binding between MuvB and p130. Following the G1 to S phase transition, the MuvB core binds to BMYB to form the MMB complex resulting in activation of mitotic genes.

Given that both BMYB and the MuvB component LIN9 are important for transcription of G2/M genes and entry into mitosis (Osterloh et al, 2007; Zhu et al, 2004), it is possible that these proteins bind to target gene promoters in a cell cycle dependent manner. Indeed, ChIP-qPCR

experiments for the MuvB component LIN54 performed at different phases of the cell cycle revealed that it binds to late cell cycle gene promoters throughout S-phase and G2. In contrast, ChIP for BMYB revealed that it is bound to late cell cycle promoters during S-phase and then diminishes from G2 to M phase (Sadasivam et al, 2012). These findings suggest that once the MuvB core is recruited to promoters in a BMYB-dependent manner, the MuvB core remains bound to these promoters after BMYB binding is lost.

BMYB protein levels are highest during S-phase and begin to decrease during G2 and M phase, which coincides with its target promoter occupancy. ChIP-qPCR experiments together with phosphatase and proteasome inhibitor studies revealed that BMYB is phosphorylated in S-phase and undergoes proteasomal degradation during G2 without disrupting the MuvB core promoter occupancy (Sadasivam et al, 2012). Furthermore, loss of BMYB binding to its target promoters precedes gene expression suggesting that another transcription factor might contribute to late cell cycle gene expression (Sadasivam et al, 2012). Like BMYB, FOXM1 is repressed by the DREAM complex in G0 and expressed during S-phase, and binds to the promoters of late cell cycle genes (Korver et al, 1997; Litovchick et al, 2007; Chen et al, 2013). Furthermore, loss of FOXM1 or BMYB results in a similar phenotype, such as delayed entry into mitosis and reduced expression of late cell cycle genes (Laoukili et al, 2005). According to co-immunoprecipitation and ChIP studies, FOXM1 interacts with the MuvB core and co-occupies target promoters during late S-phase, G2, and mitosis (Sadasivam et al, 2012). Furthermore, depletion of either BMYB or LIN9 reduces FOXM1 binding at target promoters and decreases expression of G2/M genes, indicating that the MuvB core and BMYB are required for recruiting FOXM1 to target promoters (Sadasivam et al, 2012; Down et al, 2012).

In summary, the MuvB core plays a central role in directing key transcription factors to the promoters of cell cycle-dependent genes (Figure 4). However, little is known about how the MuvB core interacts with p130 to form the DREAM complex, and how these interactions are manipulated throughout the cell cycle. Therefore, understanding the structural mechanism governing DREAM complex formation could provide insight into the regulation of cell cycle exit and progression, which is commonly perturbed in cancer.

1.6. DREAM, MMB, and cancer

The balance between the "quiescent" DREAM complex and the "proliferative" MMB complex is frequently perturbed in cancer. BMYB is frequently upregulated in tumors with poor prognosis, resulting in high expression of mitotic genes (Thorner et al, 2009; O'Connell et al, 2010; Astbury et al, 2011). Subsequently, high levels of BMYB could alter the balance between the DREAM and MMB complexes in favor of MMB formation (Figure 5). Interestingly, low levels of BMYB have also been associated with cancer, where loss of function mutations or haploinsufficiency in animal models led to mitotic defects and an increased susceptibility to cancer (Shepard et al, 2005; Clarke et al, 2013). Furthermore, the BMYB gene, *MYBL2*, is located in the 20q locus, which is frequently deleted in human myelodysplastic syndrome (MDS) (Mullier et al, 2012). The mechanism by which low levels of BMYB could lead to cancer is unclear, but is likely due to deregulated cell cycle-dependent gene expression.

Cell cycle defects such as unrestricted proliferation could be mediated by deregulation of CDK activity (reviewed in Malumbres & Barbacid, 2009). During the G1/S transition, cyclin D-CDK 4/6 complexes phosphorylate the RB family proteins to initiate normal cell cycle progression (reviewed in Giacinti & Giordano, 2006). However, cancer cells often aquire increased CDK/cyclin activity through amplification of their genes or loss of upstream inhibitors,

resulting in unscheduled cell cycle re-entry or uncontrollable proliferation (reviewed in Malumbres & Barbacid, 2009). Interestingly, previous studies showed that DREAM disassembly coincides with increased CDK4 activity during the normal G1/S transition (Pilkinton et al, 2007). Therefore, high CDK activity could lead to DREAM disassembly and increased cell proliferation through hyperphosphorylation of p130 (Figure 5).

The gene encoding DYRK1A kinase undergoes frequent loss of heterozygosity in human cancers, such as high-grade serous ovarian carcinoma (L. Litovchick, personal communication). Loss of DYRK1A activity disrupts DREAM complex assembly and reduces the ability of cells to enter quiescence resulting in uncontrolled proliferation (Litovchick et al, 2011). Therefore, loss of DYRK1A could decrease DREAM assembly resulting in increased MMB formation (Figure 5). Furthermore, in neuroblastoma cells, overexpression of DYRK1A induced cell cycle arrest and neuronal differentiation by promoting proteosomal degradation of cyclin D1 while stabilizing the CDK2 inhibitor p27 (Soppa et al, 2014). Therefore, DYRK1A could be important to counter the proliferative effects of high CDK activity.

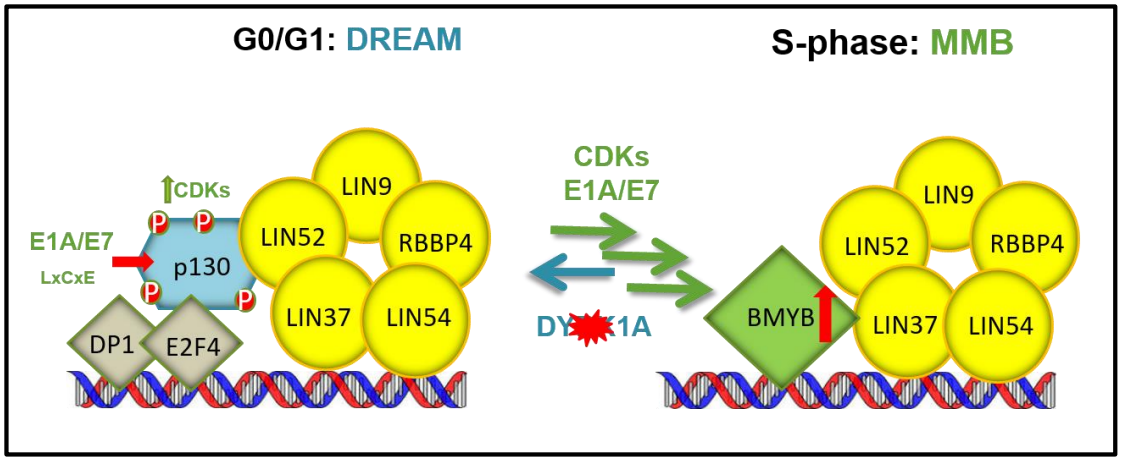

Figure 5. The DREAM complex is frequently perturbed in cancer.
Loss of DYRK1A, high CDK activity, expression of viral oncoproteins (E1A and E7), and increased expression of BMYB alters the balance between the DREAM and MMB complexes to favor MMB formation.

1.7. Viral proteins, DREAM and cancer

Small DNA tumor viruses such as such as human papillomaviruses (HPV), Simian virus 40 (SV40) and adenovirus were reported to cause tumor formation in several animal models (reviewed in Javier & Butel, 2008; DeCaprio, 2009). Consequently, the disturbing observation that several polio vaccine stocks were contaminated with SV40 led to an intense investigation of these small DNA tumor viruses, which resulted in many important advances in the field of molecular biology (reviewed in Poulin & DeCaprio, 2006).

Given the small size of the viral genomes, it was relatively simple to map their transforming genes, which led to the discovery of protein products, termed 'oncoproteins', such as adenovirus E1A, HPV E7, and SV40 large T antigen (LT) (reviewed in Moran, 1993; Felsani et al, 2006; DeCaprio, 2009). The observation that E1A and LT could bind to cellular proteins provided insight into their ability to transform cells, and aided in the discovery of RB function (reviewed in Javier & Butel, 2008). Adenovirus E1A was the first viral oncoprotein found to bind to a phosphorylated protein known as RB (reviewed in Helt & Galloway, 2003). Furthermore, LT and E1A were found to preferentially bind to the hypophosphorylated or G0/G1 form of RB, resulting in the progression from G1 to S phase. These results suggested that hypophosphorylated RB serves as a growth suppressor that can be inactivated by these viral oncoproteins (reviewed in DeCaprio, 2009). Soon after these observations many laboratories sought to identify other proteins that could bind to E1A and LT, which led to the discovery of the RB-like proteins, p107 and p130 (reviewed in DeCaprio, 2009).

A highly conserved LxCxE sequence motif was identified in each viral oncoprotein (Figure 6A). Interestingly, a small peptide containing the HPV E7 LxCxE motif was enough to compete with E2F for RB binding, suggesting that the LxCxE sequence is critical for interacting with RB (reviewed in Felsani et al, 2006; DeCaprio 2009). It was later discovered that E1A, LT and E7 use the LxCxE motif to target the pocket domain of the RB family members, leading to inactivation of RB followed by activation of E2F dependent transcription (Figure 6B) (reviewed in Helt & Galloway, 2003). In addition, more recent studies found that HPV E7 can bind to p130 resulting in disruption of the DREAM complex followed by cell cycle progression (reviewed in DeCaprio, 2014). However, exactly how viral oncoproteins displace p130 from the MuvB core remains to be elucidated.

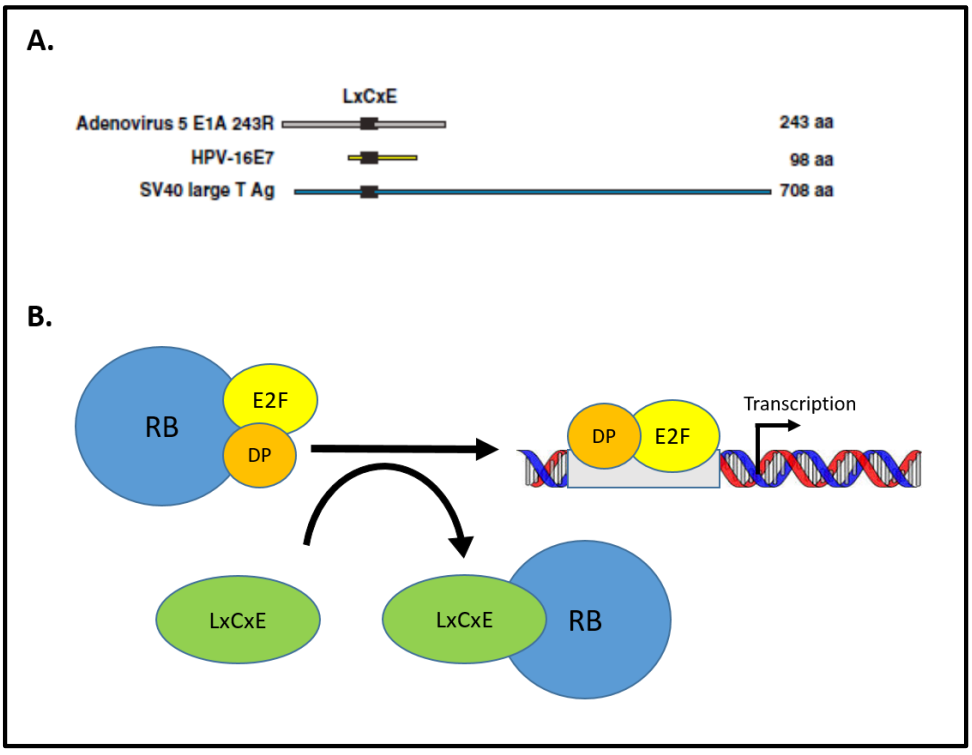

Figure 6. Viral oncoproteins contain an LxCxE motif to inactivate RB.
(A) Schematic of viral oncoproteins aligned at the LxCxE motif (Adapted from Felsani, et al. 2006). (B) Viral oncoproteins (green oval labeled LxCxE) use an LxCxE motif to bind and inactivate RB family members resulting in E2F dependent transcription.

1.8. Goals

The goals of our study are to characterize the structural and functional determinants of DREAM assembly and disassembly. Lack of progress in controlling tumor cell proliferation and overcoming cancer dormancy is largely due to our poor understanding of cell cycle exit pathways. Given that cell cycle exit and cell cycle-dependent gene expression are frequently perturbed in cancer, it is critical to characterize the molecular mechanisms that govern entry into G0/G1. Overall, our study will significantly advance our knowledge of cell cycle regulation, while unveiling new therapeutic strategies to halt tumor cell proliferation.

CHAPTER 2: MATERIALS AND METHODS

2.1. Cell culture

Established T98G, U-2 OS, HeLa, and Phoenix cell lines were obtained from the American Type Culture Collection (ATCC). BJ-hTERT fibroblasts that stably express HA-Flag tagged green fluorescent protein (GFP) or BMYB were previously generated by L. Litovchick. Mouse embryonic fibroblasts (MEFs) that stably express SV40LT-pBabe were kindly provided by S. Grossman. Cell lines were grown under sterile conditions in a 37°C incubator with 5% CO2 in the Dulbecco's modified medium (DMEM, Corning Cat# 15-013-CV) supplemented with 1% (v/v) GlutaMax (Life Technololgies, Cat# 35050-61), 1% (v/v) Penicillin/Streptomycin (Corning, Cat# 30-002CI) and 10% (v/v) FBS (Atlanta Biology, Cat# S11150). For passaging, cells were washed once with 1X PBS (Corning, Cat# MT21-031-CV), detached using 0.25% Trypsin/EDTA (Gibco, Cat# 25200-056) followed by re-suspension in fresh growth medium. The cells were counted using a hemocytometer (Hausser Scientific) and seeded into 10 cm, 6-well or 96-well tissue culture plates according to the experimental protocols.

2.2. Cell treatments and reagents

For T98G serum deprivation experiments, 500,000 cells were seeded onto 10 cm dishes and allowed to attach for 24 h. Then, growth medium was aspirated and replaced with serum-free DMEM containing 1% GlutaMax, 1% Penicillin/Streptomycin for indicated time points. For CDK4/6 inhibitor treatments, T98G cells were serum-starved for 72h, released in DMEM

containing 10% FBS with or without the CDK 4/6 inhibitor palbociclib at 0.5 μM (gift of S. Rubin), and harvested at the indicated time points.

2.3. Plasmids and mutagenesis

The HA-Flag-tagged GFP and LIN52 pMSCV retroviral constructs and LIN52-V5-pEF6 construct as well as S28A-LIN52 mutant versions were previously generated by L. Litovchick. , The LT- and E1A-pBabe constructs were provided by S. Grossmann. The wild type and T401A/T417A (TTAA) mutant HA-p130-pcDNA3.1 constructs were provided by S. Rubin. The E22A and S20C LIN52-pMSCV-CTAP constructs were generated using a QuikChange II XL Site-Directed Mutagenesis kit (Agilent Technologies, Cat# 200521) according to the manufacturer's protocol.

2.4. Production of retroviral particles

pMSCV-CTAP retroviral vectors encoding GFP, wild type LIN52, or mutant LIN52 were used for the production of virus condition medium (VCM) by transfecting Phoenix packaging cells. For each transfection, 200,000 cells per well were plated onto six-well plates in 2.5mL of complete medium and allowed to attach overnight. Cells were then transfected with 2 μg of pMSCV plasmid containing the gene of interest together with 0.1 μg pCMV-GagPol packaging plasmid and 0.1 μg pCMV-VSVG envelope plasmid. OptiMEM medium (Life Technologies, 31985070) and TransIT2020 Mirus reagent (Mirus Bio, Cat# MIR 5400) were used for the transfection according to the manufacturer's protocol. The VCM was collected 48 and 72 hours post transfection and centrifuged at 2000rpm at 4°C for 10 minutes to collect the supernatant devoid of the Phoenix cells. Aliquots of the VCM were made and stored at -80°C.

2.5. Generation of stable cell lines

The VCM was allowed to thaw overnight at 4°C. T98G, MEFs, or HeLa cells were plated onto six-well plates at 50,000 cells per well and allowed to attach overnight. Next, the medium was aspirated from each well and replaced with 1mL of fresh medium containing polybrene (8µg/mL) (Sigma, Cat# 107689) and 1mL of VCM. After 24h, the medium was replaced with 2mL of fresh complete DMEM medium. On the following day, the cells were subjected to antibiotic selection by replacing the medium with medium containing 1µg/mL Puromycin (Gold Biotechnology, Cat# P-600-100). The selection process was continued for 1 week.

2.6. Transient transfections

The established U-2 OS cell lines were co-transfected with HA-tagged wild type or TTAA mutant p130 and V5-tagged LIN52 using Mirus TransIT2020 reagent and OPTI-MEM according to the manufacturer's protocol using 200,000 cells and 1µg of DNA per well of a 6-well plate or 750,000 cells and 8µg DNA per 10cm dish. T98G cells that stably express wild type or mutant LIN52 were either transfected with empty vector-, E1A-, or LT- pBabe as described above using 750,000 cells and 8µg DNA per 10cm dish. At 48 hours post transfection, the cells were lysed directly on the plate using EBC buffer (50 mM Tris-HCl pH 8.0, 5mM EDTA, 120 mM NaCl and 0.5% NP-40) supplemented with protease inhibitors (1:100), phosphatase inhibitors (1:500) and β-ME (1:10,000) and used for immunoprecipitation and Western blot analysis.

2.7. Preparation of cell extracts

Cell lysates were typically prepared at 48h post transfection, at the indicated experimental time points or when the cells became confluent. The cells from a 10cm dish were rinsed twice with PBS and then scraped into 0.75mL of ice cold PBS containing protease

inhibitor cocktail at a dilution of 1:100 (Calbiochem, Cat#539131) and phosphatase inhibitors at a dilution of 1:500 (Calbiochem, Cat# 524625). Then, cells were collected by centrifugation and the pellets were either frozen at -80°C or lysed immediately. Cell lysis was performed using EBC buffer supplemented with protease inhibitors (1:100), phosphatase inhibitors (1:500) and β-ME (1:10,000). The lysates were clarified by centrifugation (14,000g, 15min) and the protein concentrations were measured using the BioRad DC assay.

2.8. Immunoprecipitation

The cell extracts (0.5 – 1 ml) were adjusted to the same protein concentrations by diluting with EBC buffer. A 50-100µL aliquot of each lysate was reserved to prepare the input sample by mixing with equal volume of 2X sodium dodecyl sulfate polyacrylamide gel electrophoresis (SDS PAGE) sample loading buffer (BioRad, Cat# 161-0737) and incubating at 95°C for 5 min. The remaining lysates were incubated with mixture containing 1µg of antibody, 20µL of Protein A Sepharose beads suspension (GE healthcare, Cat# 17-0780-01), and 80µL of EBC overnight on a rocker at 4°C. Next, the beads were collected by centrifugation at 10,000g for 30 sec at 4°C and washed five times with cold EBC buffer to remove any unbound protein. After the last wash, the supernatant was aspirated and 30µL of 1X SDS PAGE sample loading buffer was added to the tubes followed by incubation at 95°C for 5 min.

2.9. Western Blotting

The samples for Western blot analysis were resolved using a 7.5% SDS-PAGE gels or a 4-20% Criterion TGX Precast gel (BioRad Cat# 567-1094) and transferred to a nitrocellulose membrane (Amersham, Cat# 10600006) using semi-dry electrophoretic transfer (45 min, 15V). The membrane was blocked for 1 hour in 3% non-fat dry milk in TBST buffer containing 1X Tris buffered saline (TBS) (Boston BioProducts, Cat# BM-300) and 0.05% Tween-20 (BioRad

Cat# 1610781). The membranes were then probed with primary antibodies diluted in the blocking buffer and incubated overnight at 4°C. The blots were developed by incubation with horseradish peroxidase (HRP) -conjugated secondary antibodies (anti-rabbit or anti-mouse) diluted in 1% milk for one hour at room temperature (RT) followed by chemiluminescence detection. Protein bands were visualized using X-ray film (Phenix, Cat# F-BX57 and F-BX810). If re-probing of the blots was required, the Restore Western reagent (Thermo Scientific, Cat# 46430) was used to strip the membranes.

2.10. Antibodies

Mouse anti-Flag antibody (Sigma-Aldrich, Cat# A2220) was used for pull down of HA-Flag tagged proteins. The rabbit anti-HA antibody (Cell Signaling, Cat# 3724S) was used for Western Blot Analysis of HA-Flag tagged proteins. Rabbit anti-p130 (Santa Cruz, Cat# SC-317), mouse anti-p130 (BD Bioscience, Cat# 610262), and samples of rabbit antibodies against LIN37, LIN9, and p130 provided by Bethyl Inc. (Litovchick et al, 2007) were used to detect components of the DREAM complex, respectively. Mouse anti-HPV18 E7 (Santa Cruz, Cat# sc-365035), anti-E1A (Santa Cruz, Cat# sc-25), and anti-SV40 T Ag (Santa Cruz, Cat# sc-147) antibodies were used for Western blot analysis of viral oncoprotein in input samples, respectively. For endogenous LIN37 pull down experiments and for immunoblotting, the rabbit anti-LIN37 antibody from Bethyl Inc. (Litovchick et al, 2007) was used. Rabbit anti-V5 antibody (Bethyl, Cat# A190-120A) was used for pull down of V5 tagged LIN52 protein, and mouse anti-V5 antibody (AbD Serotec, Cat# MCA1360GA) was used for Western blot analysis of V5-tagged LIN52 protein. Mouse anti-HA antibody (Santa Cruz, Cat# sc-7392) was used for pull down of HA-tagged p130 proteins, and rabbit anti-HA antibody was used for Western blot analysis of HA-tagged p130 proteins. An antibody only sample was used for IgG pull down controls. HRP

conjugated anti-mouse IgG (Jackson lab, Cat# 115-035-003), HRP conjugated anti-rabbit IgG (Jackson lab, Cat#111-035-003) and HRP conjugated anti-rabbit light chain IgG (Jackson lab, Cat# 211-032-171) were used as secondary antibodies for immunoblotting.

2.11. Ki-67 staining

U-2 OS cells were seeded onto six-well plates at 200,000 cells per well and transfected with pcDNA3.1 vectors encoding p130 constructs and GFP as described above. The p130 vector was transfected at a 4:1 molar ratio relative to the GFP vector. 48h post transfection, cells were trypsinized and seeded in triplicate onto six-well plates containing glass cover slips and allowed to attach for 24h. Next, cells were washed with 1X PBS and then fixed by incubating with 2 mL of 4 % paraformaldehyde (Ricca chemical company, Cat# 3191-31) for 30 min at RT. The cells were then washed with 1X PBS and permeabilized and blocked by incubating with 0.2 % Triton-X (Fisher Scientific, 9002-93-91) in 5% BSA for 30 min at RT. The coverslips were incubated with the primary antibody (rabbit anti-Ki67 (Millipore, Cat# AB9260) diluted 1:300 in the blocking buffer) under humid conditions for 1 hour at RT. The coverslips were washed three times with PBS for 10 min each and incubated with the secondary antibody (Cy3 donkey anti-rabbit IgG, Jackson lab) diluted 1:600 in the blocking buffer at RT for one hour. The coverslips were then washed as above, allowed to air dry, then mounted onto slides using mounting medium containing DAPI (Life Technologies, P36966). Images were captured using an EVOS fluorescent microscope (AMG advanced microscope group) and a 20x objective. To determine the fraction of proliferating GFP-positive (express HA-tagged wildtype and mutant p130) and GFP-negative cells, the number of Ki67-positive cells was determined in at least 100 cells per condition. To calculate statistical significance, values from triplicate experiments were analyzed using a two-tailed Student’s t-test for equal variances.

2.12. MTT assays

HeLa cells and MEFs that stably express HA-Flag tagged GFP, wild type LIN52, or mutant LIN52 were seeded in triplicate onto 96-well plates at 2500 cells per well. After 24h, 48h, and 72h time points, cells were incubated with the MTT labeling reagent and solubilized according to the manufacture's cell growth assay protocol (Roche, Cat# 11465007001). Next, absorbance was measured at 590nm using a BioTek Synergy H1 hybrid microplate reader. Proliferation was measured by an increase in metabolic activity (a surrogate measure of the cell number) at 72h relative to 24h. To calculate statistical significance, values from triplicate experiments were analyzed using a two-tailed Student's t-test for equal variances.

2.13. Clonogenic assays

HeLa cells that stably express HA-Flag tagged GFP, wild type LIN52, or mutant LIN52 were seeded in triplicate onto six-well plates at 1000 cells per well and processed 10 days post-plating. To visualize colonies, cells were washed with 1X PBS and stained with Crystal Violet solution (Sigma, Cat# HT 90132) for 15 min. Then, the plates were rinsed by dipping into a large beaker of distilled water three to four times until there was no remaining residual dye, and allowed to air dry. Plates were imaged using a Bio-Rad multi imager (ChemiDoc MP), and colonies were counted using ImageJ Colony Counter software.

CHAPTER 3: RESULTS

3.1. Phosphorylated LIN52 directly interacts with the pocket domain of p130

Background. The DREAM complex plays an important role in cell cycle-dependent gene expression. However, the biochemical mechanisms governing DREAM function and regulation are not well understood. In collaboration with Dr. Seth Rubin, we characterized the structural basis for DREAM assembly following DYRK1A phosphorylation. Previous studies show that p107 and p130 bind to the MuvB core when LIN52 is phosphorylated at S28 (Litovchick et al, 2011), therefore, LIN52 could be the critical component that mediates this interaction. Dr. Rubin's laboratory performed several binding experiments with recombinant, purified proteins, and found that purified full length LIN52 directly associates with p130 (data not shown) (Guiley, et al. 2015). Furthermore, purified LIN52 construct containing the N-terminal domain (residues 13-45, $LIN52^{13-45}$) was sufficient to successfully coprecipitate with the p130 and p107 pocket domain, whereas an S28A mutation in $LIN52^{13-45}$ reduced binding to p130 and p107 (data not shown) (Guiley, et al. 2015). Consistent with previous studies, the S28 phosphorylation is important to form a direct interaction with LIN52 and p130. Given that the RB family pocket domain contains an LxCxE cleft that binds to proteins containing an LxCxE sequence motif (reference), we hypothesized that LIN52 directly binds to the LxCxE cleft. In support of this, binding data revealed that purified $LIN52^{13-45}$ was unable to bind to a purified p107 pocket domain mutant (data not shown) (Guiley, et al. 2015).

To identify the molecular interactions involved in DREAM assembly and to determine the role of the LxCxE cleft of pocket proteins in LIN52 binding, Dr. Rubin's laboratory solved the crystal structure of the p107 pocket domain bound to a phosphorylated S28 LIN52[13-45] peptide or to an HPV E7 peptide. Consistent with the coprecipitation data, it was found that LIN52 binds the LxCxE cleft of p107 (Figure 7) (Guiley, et al. 2015). Interestingly, the LIN52 peptide binds to p107 using an LxSxExL motif that is similar to the canonical LxCxE sequence motif found in E7.

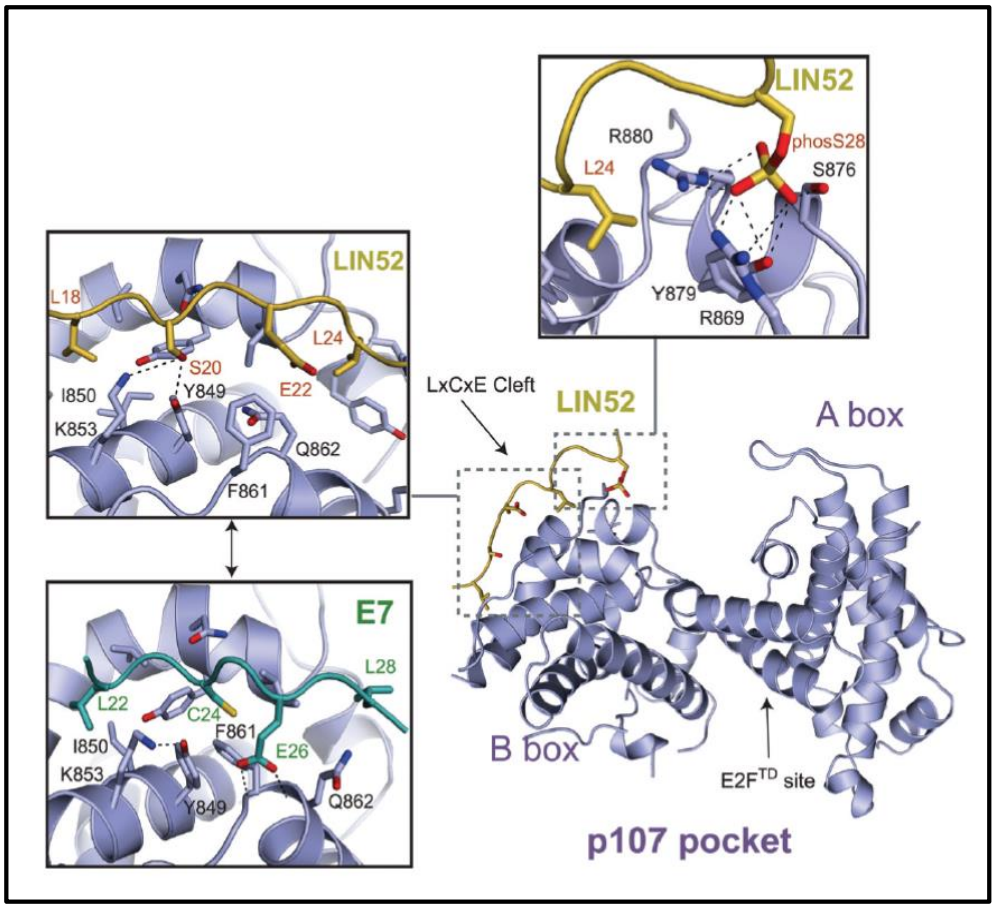

Figure 7. Crystal structure of the p107 pocket domain complexed with phosphorylated S28 LIN5212-34 or E7.
The phosphorylated S28 LIN52 peptide binds at the LxCxE cleft of the p107 pocket domain with an LxSxExL sequence motif that is similar to the E7 peptide. (Adopted from Guiley, et al., 2015)

The presence of the cysteine 24 (C24) residue within the E7 LxCxE motif and the serine 20 (S20) residue in LIN52 LxSxE motif had significant structural implications. Indeed, C24 in the E7 protein interacts with p107 backbone in a way that allows an additional hydrogen bond formation by the glutamic acid 26 (E26) side chain of E7 that was absent in LIN52-p107 complex (Figure 7) (Guiley, et al. 2015). Using isothermal titration calorimetry (ITC), Dr. Rubin's laboratory confirmed that the LIN52 LxSxExL motif binds the p107 pocket domain with weaker affinity than the canonical E7 LxCxExL motif and requires phosphorylation of S28 to stabilize the LIN52-p107/p130 complex. Therefore, LIN52 uses a suboptimal LxSxExL sequence along with phosphorylated S28 to bind to the pocket domain of p130 and p107 in a manner that can be regulated by S28 residue phosphorylation.

3.2. The LIN52 LxSxExL sequence is critical for DREAM assembly

Next, we sought to confirm the structural findings by testing the protein-protein interactions in human cells. The LIN52 LxSxExL motif along with S28 is highly conserved (Figure 8A), therefore, these residues might be important for DREAM assembly in cells. To test this, we generated dual tagged LIN52-HA-Flag mutants that were stably expressed in T98G cells (Figure 8B). To induce DREAM assembly, the LIN52 wild type and mutant expressing T98G cells were serum starved for 48h. Next, we performed immunoprecipitation using an anti-Flag antibody and examined the coprecipitation of p130 by Western blot. When either LIN52 E22 or S28 is mutated to an alanine, p130 binding is diminished, while binding of the MuvB proteins LIN37 and LIN9 remained intact (Figure 8C). As a result, both the LIN52 LxSxExL motif and

S28 phosphorylation are required for DREAM assembly, which is consistent with Dr. Rubin's crystal structure and *in vitro* binding data.

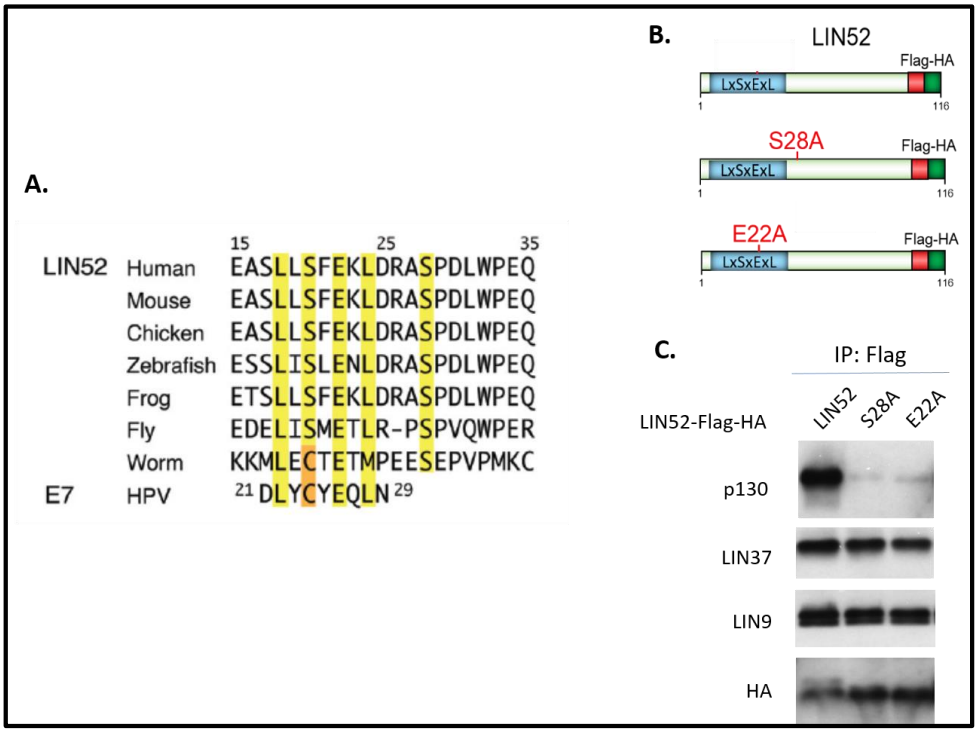

Figure 8. Both the LIN52 LxSxExL motif and S28 phosphorylation are required for DREAM assembly.
(A) Alignment of LIN52 and E7 protein sequences. The LIN52 LxSxExL and pS28 residues are highlighted (Adopted from Guiley, et al., 2015). (B) A schematic of the dual tagged LIN52-pMSCV-CTAP constructs. Each mutation is shown in red and the LxSxExL sequence is highlighted in blue. (C) T98G cells stably expressing the wild type or mutant LIN52-Flag-HA alleles were serum starved for 48h, extracts were immunoprecipitated with an anti-Flag antibody, and proteins were detected with the indicated antibodies in a Western blot.

3.3. The weaker LIN52 LxSxExL sequence enables DREAM disassembly by viral oncoproteins

Viral oncoproteins have an LxCxE sequence motif that enables them to inactivate the RB family proteins by binding to the same pocket as LIN52 (reviewed in Helt & Galloway, 2003) (Figure 9A). In addition, Dr. Rubin's ITC data suggests that the weaker LIN52 LxSxExL

sequence enables competitor viral oncoproteins to displace the MuvB core from p130. Indeed, when the LIN52 S20 residue is replaced with cysteine to mimic the canonical LxCxE motif, the LIN52 peptide binds to p107 with a similar affinity as E7 (data not shown) (Guiley, et al. 2015). Therefore, we hypothesized that mutating S20 within the LIN52 LxSxExL sequence to mimic the canonical LxCxE motif would stabilize the DREAM complex in the presence of viral oncoproteins (Figure 9A). To test this, we transiently expressed viral proteins SV40 large T antigen (LT) or adenovirus E1A in cycling T98G cells that stably express dual tagged wild type or S20C mutant LIN52 (Figure 9B). To observe differences in DREAM assembly, we performed immunoprecipitation using an anti-Flag antibody and examined the co-precipitation of p130 by Western blot. The S20C mutant expresses at a higher level than wild type LIN52 and coprecipitates greater amounts of p130. Importantly, greater amounts of p130 were also co-precipitated with LIN52-S20C in the presence of either E1A or LT than with the wild type LIN52 (Figure 9C), suggesting that the S20C mutation allows LIN52 to better compete with E1A and LT for p130 binding.

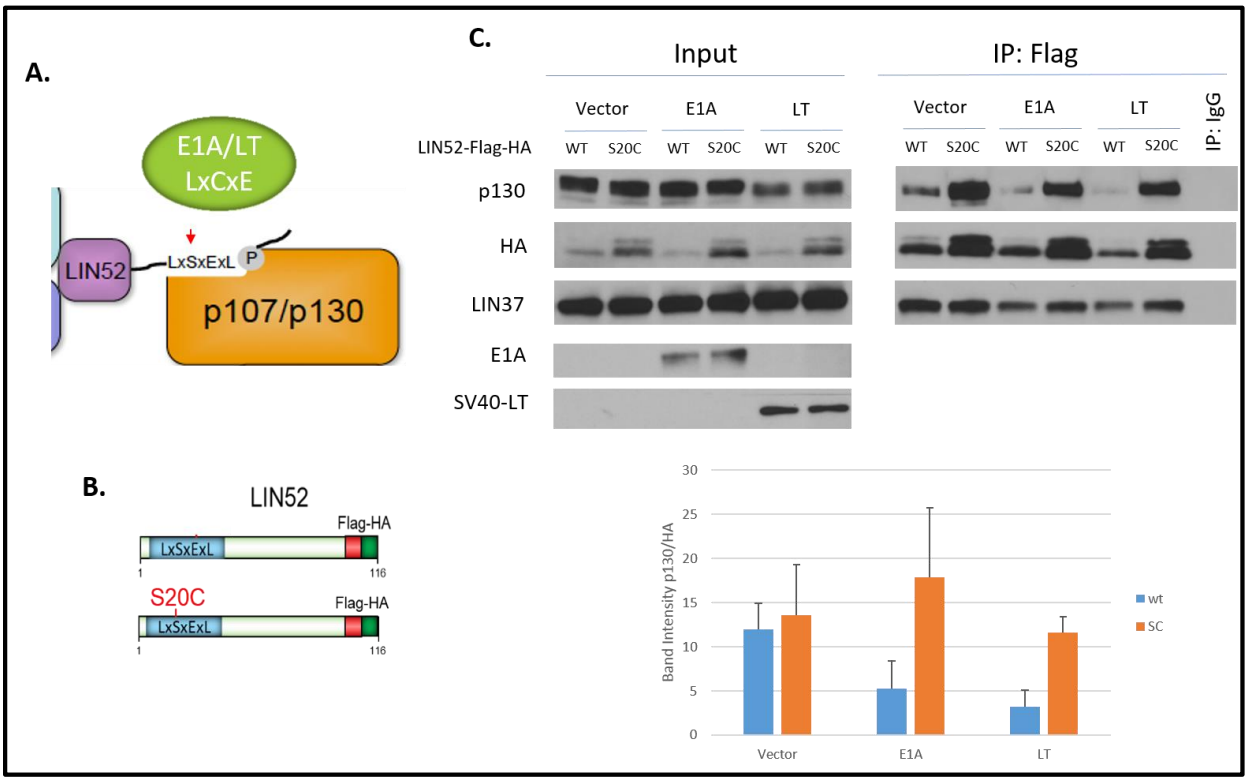

Figure 9. The weaker LIN52 LxSxExL sequence enables DREAM disassembly by viral oncoproteins.
(A) A schematic drawing of phosphorylated LIN52 binding to the p107/p130 pocket domain through an LxCxE-like motif. The red arrow indicates the S20 residue in LIN52 that was mutated to cysteine to mimic the canonical LxCxE motif. (B) A schematic of the LIN52-pMSCV-CTAP constructs used in the experiment (C) T98G cells that stably express wild type or S20C-LIN52-Flag-HA were transiently transfected with SV40 large T antigen (LT) and adenovirus E1A constructs. Extracts were immunoprecipitated with an anti-Flag antibody, and proteins were detected with the indicated antibodies in a Western blot. Band intensities for the immunoprecipitated HA-LIN52 and p130 were quantified, and the p130/HA ratio is plotted. Error bars show standard deviations for two different replicates.

3.4. The LIN52 S20C mutant reduces the proliferative effects of viral oncoproteins

Given that viral oncoproteins can disrupt DREAM (Figure 9C) and enhance cellular proliferation (Rashid et al, 2011) we hypothesized that the LIN52 S20C mutant could reduce the proliferative effects of viral oncoproteins by stabilizing the DREAM complex. To test this, we stably expressed LT together with either wild type or S20C mutant LIN52-Flag-HA in normal mouse embryonic fibroblasts (MEFs). To confirm that the ability of S20C-LIN52 to stabilize the DREAM complex is recapitulated in the MEFs, we performed immunoprecipitation using an anti-Flag antibody and examined the co-precipitation of p130 by Western blot. Unlike wild type LIN52, the S20C mutant is able to co-precipitate p130 in the presence of LT. As seen before (Fig. 9), the S20C mutant expresses at higher levels than wild type LIN52 but it does not co-precipitate greater amounts of the MuvB subunit LIN37 (Figure 10A). Furthermore, the wild type and mutant LIN52 MEF cell lines express equal amounts of SV40-LT (Figure 11).

To measure changes in cellular proliferation, we performed an MTT assay that quantifies the metabolic activity of viable cells and serves as a surrogate measure of cell number. In MEFs that stably express LT and wild type or S20C mutant LIN52, an MTT assay was performed at 24 and 72 hours after plating. To quantify changes in proliferation, a fold change in metabolic activity was calculated at 72 hours relative to 24 hours. Interestingly, expression of either wild type or S20C mutant LIN52 significantly reduced proliferation of MEFs expressing LT (Figure 10B). Since expression of the wild type LIN52 did not increase the DREAM complex formation in the MEFs expressing LT, it is possible that decreased proliferation in these cells is due to an increased MMB complex formation and deregulation of the G2/M gene expression.

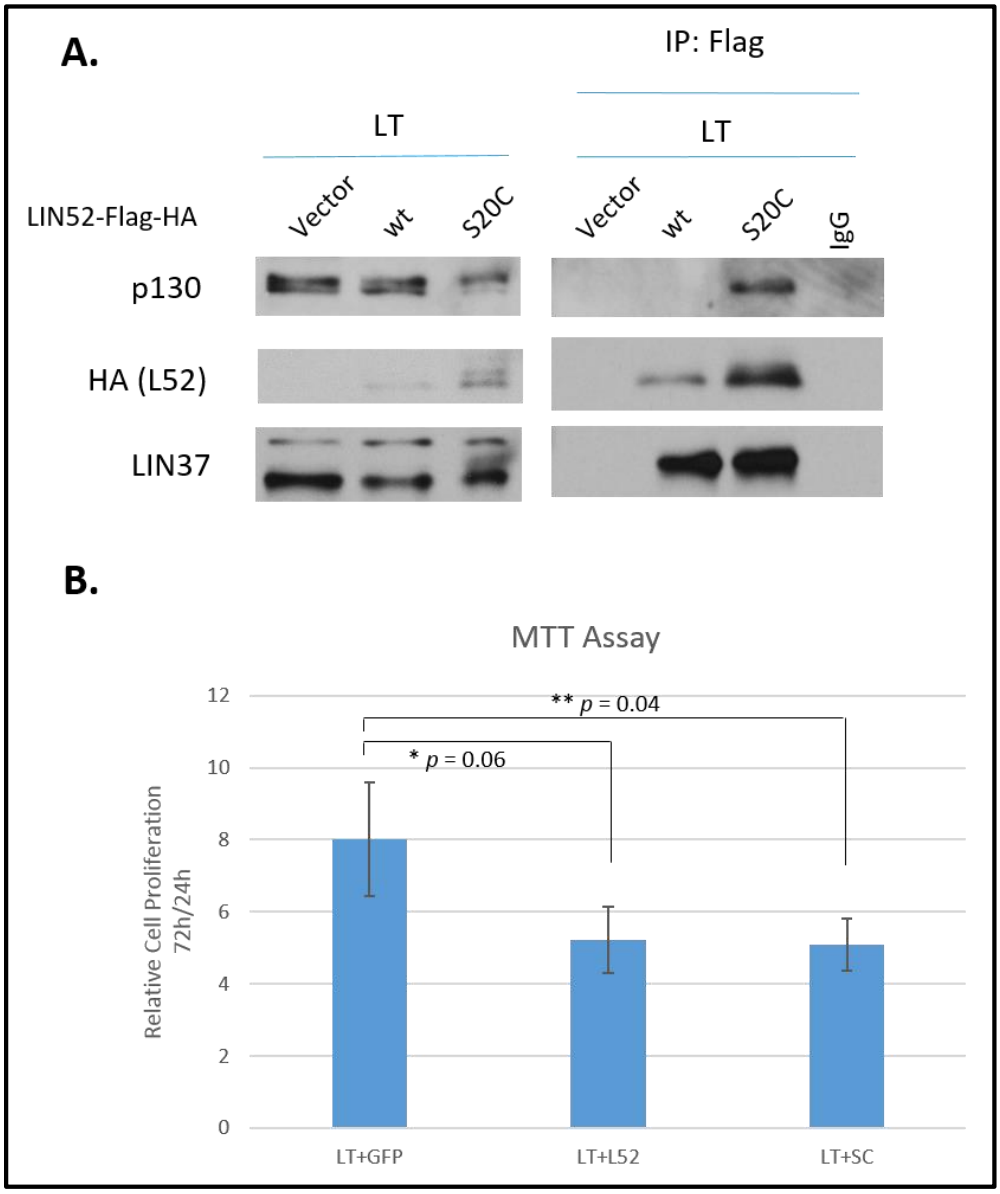

Figure 10. In the presence of SV40-LT, the LxCxE LIN52 mutant enhances DREAM assembly and alters cellular proliferation.
(A) Extracts from MEFs stably expressing SV40 large T antigen (LT) and wild type (wt) or S20C mutant LIN52-Flag-HA were immunoprecipitated with an anti-Flag antibody, and proteins were detected with the indicated antibodies in a Western blot. (B) MTT assay of MEFs stably expressing LT and wt or S20C mutant LIN52-Flag-HA. Proliferation was measured by an increase in metabolic activity at 72 h relative to 24h. Error bars are standard deviations for three biological replicates, and P-values were calculated using a two-tailed Student's t-test.

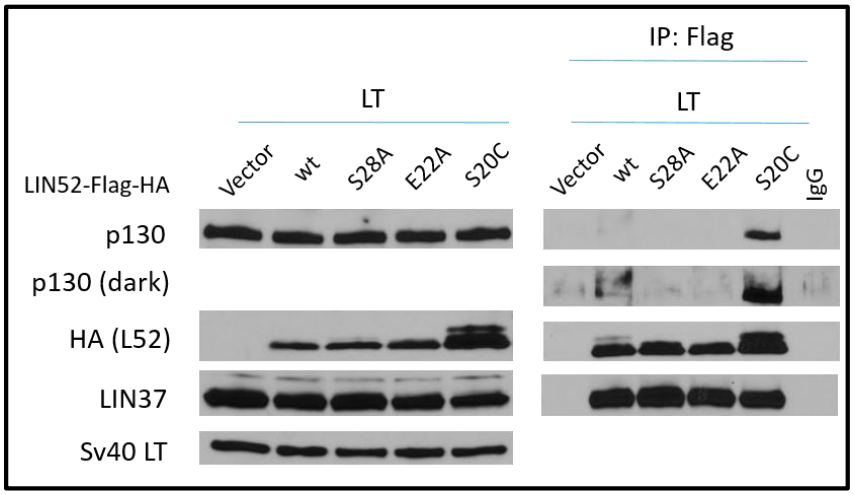

Figure 11. SV40-LT is equally expressed in MEF cell lines stably expressing different LIN52 alleles.
(A) Extracts from MEFs stably expressing SV40 large T antigen (LT) and wild type (wt) or mutant LIN52-Flag-HA were immunoprecipitated with an anti-Flag antibody, and proteins were detected with the indicated antibodies in a Western blot.

In human cervical cancer cell lines, the HPV16 E7 oncoprotein disrupts the DREAM complex to induce cell cycle progression and proliferation (Rashid, et al. 2011; DeCaprio, 2014). Due to the presence of HPV18 E7, cervical adenocarcinoma HeLa cells do not have a detectable DREAM complex compared to normal cells and other cancer cell lines such as T98G (Sadasivam, et al, 2012). Therefore, we hypothesized that our LIN52 S20C mutant could restore DREAM assembly and reduce cellular proliferation in HeLa cells. To test this, we first stably expressed dual tagged wild type or S20C mutant LIN52 in HeLa cells and performed immunoprecipitation using an anti-Flag antibody. To observe changes in DREAM assembly, we examined the co-precipitation of p130 by Western blot. Unlike wild type LIN52, the S20C mutant was able to co-precipitate p130. As previously seen in T98G cells and MEFs, the S20C mutant expresses at higher levels than wild type LIN52 but it does not co-precipitate greater amounts of the MuvB subunit LIN37 (Figure 12A).

To determine if S20C-LIN52 can affect HeLa cell proliferation, we performed MTT and clonogenic assays. The metabolic activity of HeLa cells that stably express wild type or S20C

mutant LIN52 was measured at 24 and 48 after plating. To quantify changes in proliferation, a fold change in metabolic activity was calculated at 48 hours relative to 24 hours. Although both the wild type LIN52 and the S20C mutant reduced proliferation of HeLa cells in this assay, the difference was significant only in case of ectopically expressed S20C mutant LIN52 (Figure 12B). A clonogenic assay was performed in HeLa cells that stably express wild type or S20C mutant LIN52 as an additional method to measure cellular proliferation. In support of the MTT assay result, S20C-LIN52 again significantly reduced the ability of HeLa cells to form colonies while the wild type LIN52 showed no effect (Figure 13A & B). Together, these results demonstrate that mutating LIN52 to mimic the canonical LxCxE motif restores DREAM assembly and reduces cellular proliferation in the presence of viral oncoproteins.

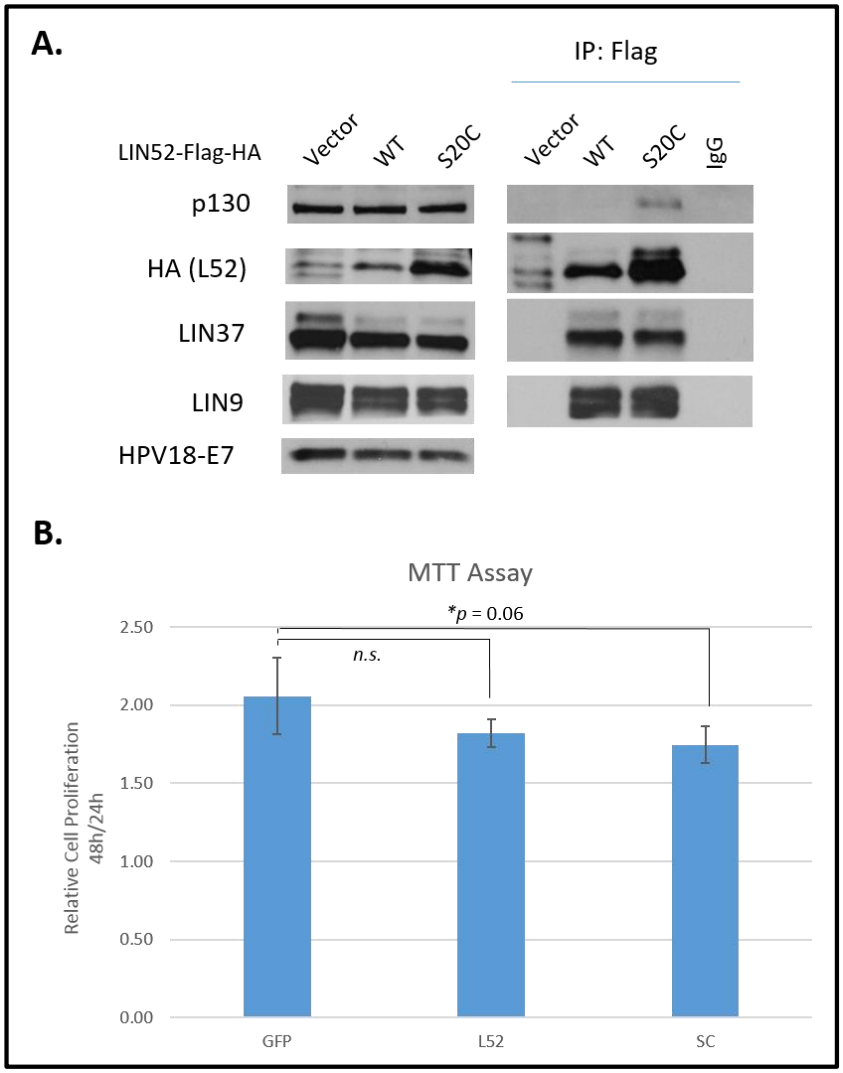

Figure 12. The LxCxE LIN52 mutant restores DREAM assembly and reduces cellular proliferation in HeLa cells.
(A) Extracts from HeLa cells stably expressing wild type (wt) or S20C mutant LIN52-Flag-HA were immunoprecipitated with an anti-Flag antibody, and proteins were detected with the indicated antibodies in a Western blot. (B) MTT assay using HeLa cells stably expressing wt or S20C mutant LIN52-Flag-HA. Proliferation was measured by an increase in metabolic activity at 48h relative to 24h. Error bars are standard deviations for three biological replicates, and P-values were calculated using a two-tailed Student's t-test.

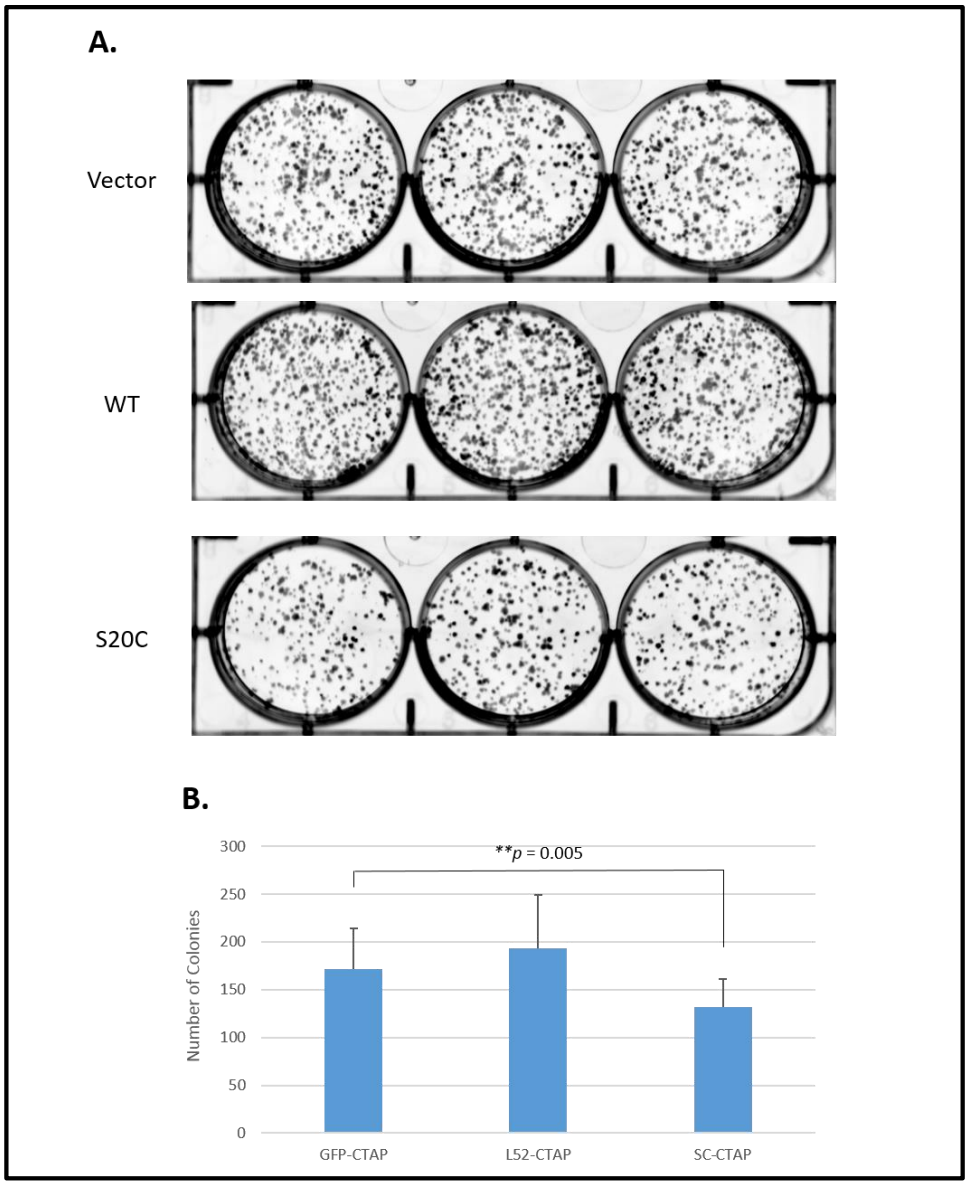

Figure 13. The LxCxE LIN52 mutant reduces colony formation in HeLa cells.
(A) HeLa cells stably expressing wild type (wt) or S20C mutant LIN52-Flag-HA were seeded in triplicate onto 6-well plates at 1000 cells per well and processed 10 days post-plating. Colonies were stained with Crystal Violet and imaged using a Bio-Rad multi imager. Representative images are shown. (B) Colonies were counted using ImageJ Colony Counter software. Error bars are standard deviations for three biological replicates, and P-values were calculated using a two-tailed Student's t-test.

3.5. CDK activity contributes to DREAM disassembly

The MuvB complex fails to associate with p107 and p130 in cycling cells, however, the mechanism of DREAM disassembly upon cell cycle entry has not been elucidated. Given that LIN52 binds to BMYB both in its phosphorylated and unphosphorylated form (Litovchick et al. 2011), dephosphorylation of LIN52 S28 is unlikely to be the primary mechanism of DREAM disassembly. Previous studies show that DREAM disassembly coincides with increased CDK 4/6 activity (Pilkinton et al, 2007), therefore, we hypothesized that CDK 4/6 phosphorylation of p130 results in DREAM disassembly. To test whether CDK activity directly correlates with p130 binding to MuvB, we performed immunoprecipitation in cycling T98G cells using an anti-LIN37 antibody in the presence or absence of a CDK4/6 inhibitor palbociclib. According to Western blot analysis, the MuvB component LIN37 co-precipitates greater amounts of p130 in the presence of the CDK4/6 inhibitor (Figure 14A). To test the effect of CDK inhibition on DREAM disassembly upon cell cycle entry, we serum starved T98G cells for 72 hours and released them in 10% FBS in the absence or presence of the CDK4/6 inhibitor. After harvesting cells at the indicated time points, changes in DREAM assembly were monitored by immunoprecipitation using an anti-LIN37 antibody followed by a Western blot. We found that the co-precipitation of LIN37 and p130 persists to a greater extent in the presence of the CDK 4/6 inhibitor, whereas in the absence of the inhibitor, the loss of p130 co-precipitation correlates with the appearance of hyperphosphorylated p130 (Figure 14B). Together, these results demonstrate that CDK activity contributes to the DREAM disassembly in cycling cells.

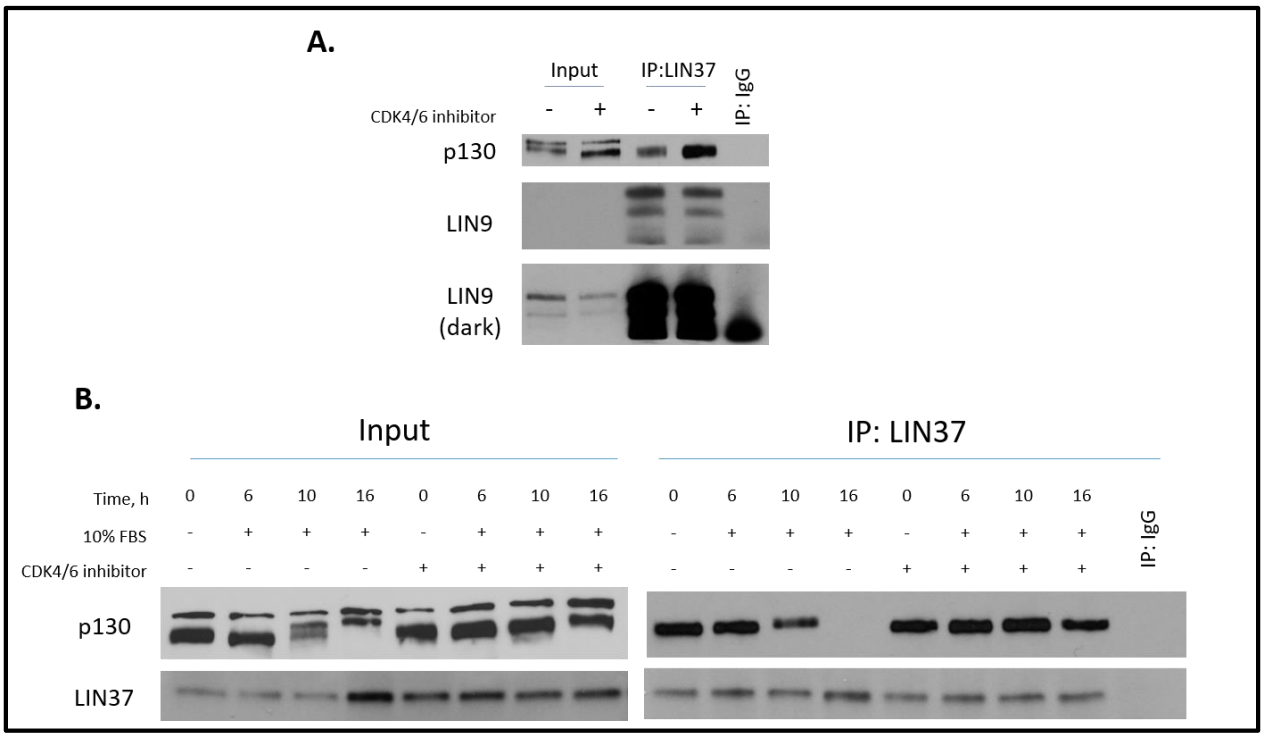

Figure 14. p130 phosphorylation by CDK 4/6 promotes DREAM disassembly.
(A) T98G cells were incubated for 24h in the presence or absence of a CDK4/6 inhibitor palbociclib (0.5 μM). Binding of p130 to LIN37 was determined by co-immunoprecipitation with an anti-LIN37 antibody and probed for p130 and LIN9. (B) T98G cells were serum-starved for 72h and released in 10% FBS in the absence or presence of the CDK4/6 inhibitor palbociclib. After harvesting cells at the indicated time points, extracts were immunoprecipitated with an anti-LIN37 antibody and probed for LIN37 and p130.

p130 has several CDK phosphorylation sites that are important for controlling cell cycle progression. The interdomain linker within the p130 pocket domain contains two CDK phosphorylation sites T401 and T417 that could play a role in DREAM disassembly (Hansen et al., 2001; Guiley et al., 2015). Given that the p130 pocket domain is essential for MuvB binding (Guiley et al., 2015), we wanted to determine whether CDK phosphorylation disrupts the DREAM complex through phosphorylation of residues within the p130 interdomain linker (Figure 15A). To test this, we generated a T401A/T417A (TTAA) p130 phosphosite mutant and examined its effect on MuvB binding. In cycling U-2 OS cells, we expressed wild type V5-tagged LIN52 together with HA-tagged p130 wild type or the double phosphosite mutant. Next,

we performed immunoprecipitation using an anti-V5 antibody and found that LIN52 co-precipitates greater amounts of the TTAA p130 mutant (Figure 15B). Furthermore, we performed a reverse immunoprecipitation using an anti-HA antibody and confirmed that the TTAA mutant can co-precipitate greater amounts of endogenous LIN37 than wild type p130 (Figure 15C). Together these results show that CDK phosphorylation sites within the interdomain linker are important for disrupting the DREAM complex.

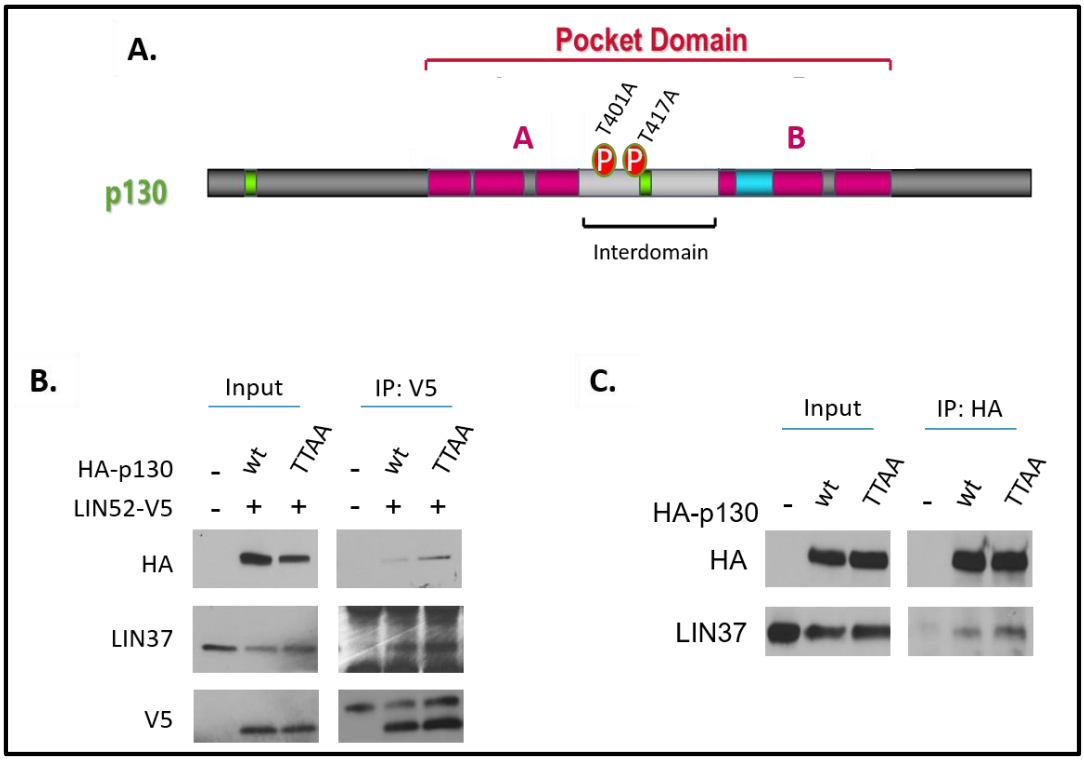

Figure 15. Disrupting p130 CDK 4/6 phosphorylation sites enhances DREAM assembly. (A) To determine whether CDK phosphorylation disrupts the DREAM complex, specific phosphorylation sites within the interdomain were mutated. (B) U-2 OS cells were transiently transfected with LIN52-V5 and the wild type (WT) or T401A/T417A (TTAA) mutant HA-p130. Extracts were immunoprecipitated with anti-V5 antibody, and the indicated proteins were detected by Western blot. (C) Same as in B except the reverse pull-down was performed using an anti-HA antibody

To determine the functional consequences of mutating the T401 and T417 CDK phosphorylation sites, we transfected cycling U-2 OS cells with either wild type p130 or the

TTAA-p130 mutant and GFP as a tracer. Next, we examined alterations in cellular proliferation through Ki-67 immunofluorescence staining (Figure 16A). Ki67 is a protein present during all the phases of the cell cycle except for G0 making it an excellent proliferation marker (Scholzen & Gerdes, 2000). In cells that ectopically express wild type or mutant p130 (GFP-positive cells), the percentage of proliferating cells (Ki-67 positive) is reduced compared to cells lacking the p130 constructs (GFP-negative). Furthermore, expression of the TTAA-p130 significantly reduced the percentage of proliferating U-2 OS cells (Ki-67 positive cells) compared to wild type p130 (Figure 16B). Therefore, disrupting the T401/T417 CDK phosphorylation sites results in a more potent growth arrest by p130 that is consistent with stabilization of the DREAM complex.

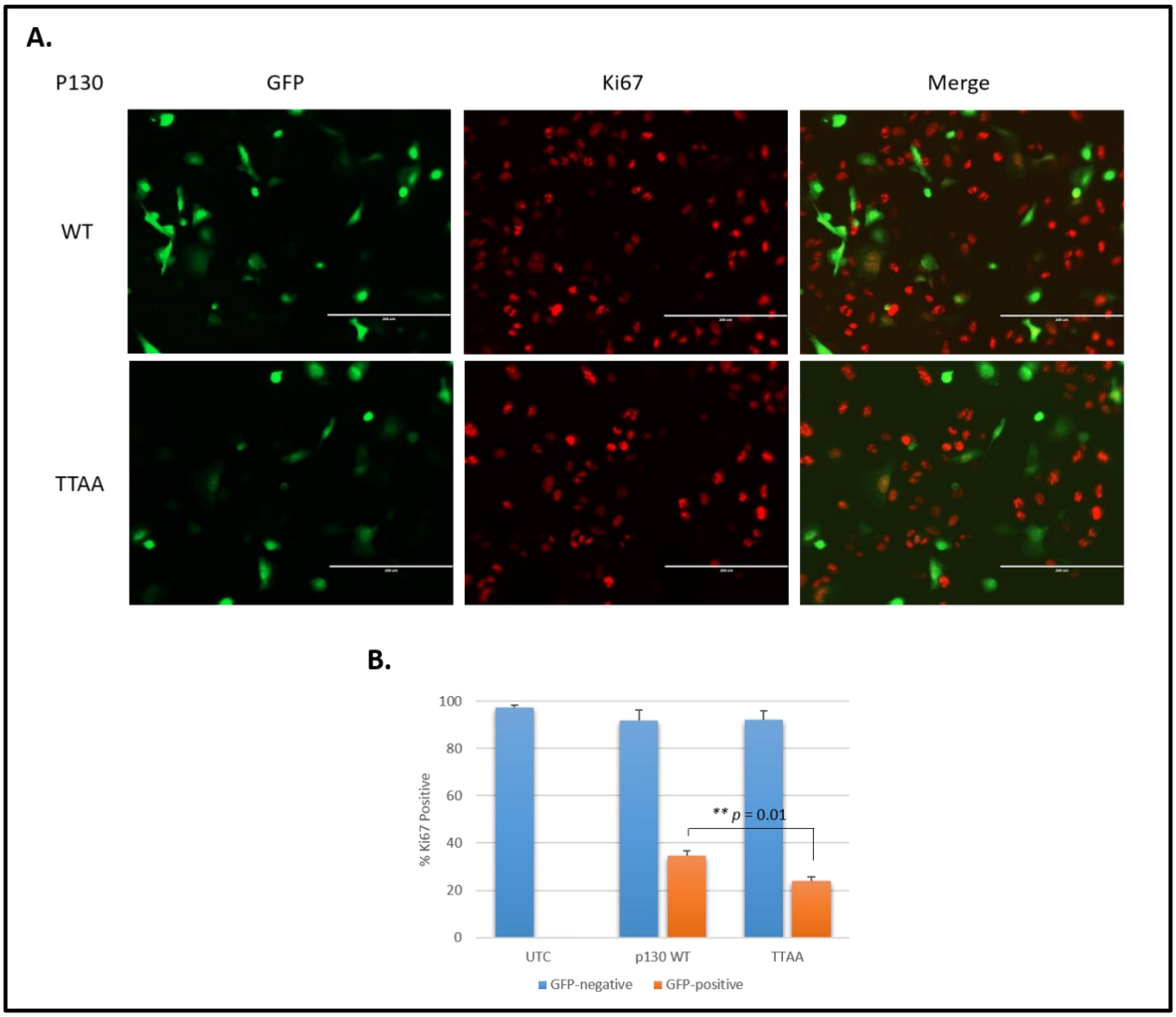

Figure 16. Disrupting p130 CDK 4/6 phosphorylation sites enhances DREAM function. (A) U2-OS cells were transiently co-transfected with wild type (WT) or T401A/T417A (TTAA) mutant HA-p130 and GFP as a tracer (green). The expression of Ki-67 (red) was determined by indirect immunofluorescence cell staining at 48h after transfection. Representative images at 20X are shown. (B) The graph shows the average values and standard deviations (error bars) of three replicate experiments where at least 100 cells were counted per condition. The significant P-value was calculated using a two-tailed Student's t-test.

3.6. p130 and BMYB bind different surfaces of MuvB

Previous studies suggested that binding if human BMYB and p130 to the MuvB core is mutually exclusive, while their *D. melanogaster* homologues can form a complex together (Litovchick et al, 2007; Georlette, 2007; Lewis, 2004). To compare the mechanisms of DREAM and MMB assembly through BMYB-MuvB binding, Dr. Rubin's laboratory performed a series of co-precipitation experiments using human recombinant proteins (data not shown). He found that the C terminus of BMYB co-precipitates the p130 pocket only if the components of the MuvB core are present, which demonstrates that BMYB, MuvB, and the p130 pocket can be present as a single complex. BMYB is not expressed in G0/G1 cells when DREAM is assembled (Litovchick et al, 2007). Therefore, to determine whether full-length p130 and BMYB associate together with MuvB in cells, we stably expressed HA-Flag-BMYB in BJ-hTERT fibroblasts and performed immunoprecipitation using an anti-Flag antibody followed by Western blot analysis. To promote DREAM assembly, we either serum starved or treated cells with the CDK4/6 inhibitor palbociclib. According to Western blot analysis, BMYB only co-precipitates endogenous p130 and the MuvB component LIN37 under conditions that support DREAM assembly (Figure 17A). Together these results demonstrate that under certain conditions human p130 and BMYB can simultaneously associate with the MuvB core through non-overlapping binding sites.

Given that BMYB is upregulated in many cancers (Thorner et al, 2009; O'Connell et al, 2010; Astbury et al, 2011), we hypothesized that high levels of BMYB could perturb DREAM assembly. To test this, we immunoprecipitated endogenous LIN37 from BJ-hTERT fibroblasts that stably express HA-Flag-BMYB in the presence or absence of serum. We found that when BMYB is overexpressed in the absence or presence of serum, LIN37 co-precipitates less p130

compared to control cells (Figure 17B). Therefore, high levels of BMYB could result in reduced recruitment of p130 to the MuvB core even under conditions that favor DREAM assembly. Furthermore, this finding suggests that the simultaneous association between BMYB, p130 and MuvB could be a transition state between DREAM and MMB assembly (Figure 17C).

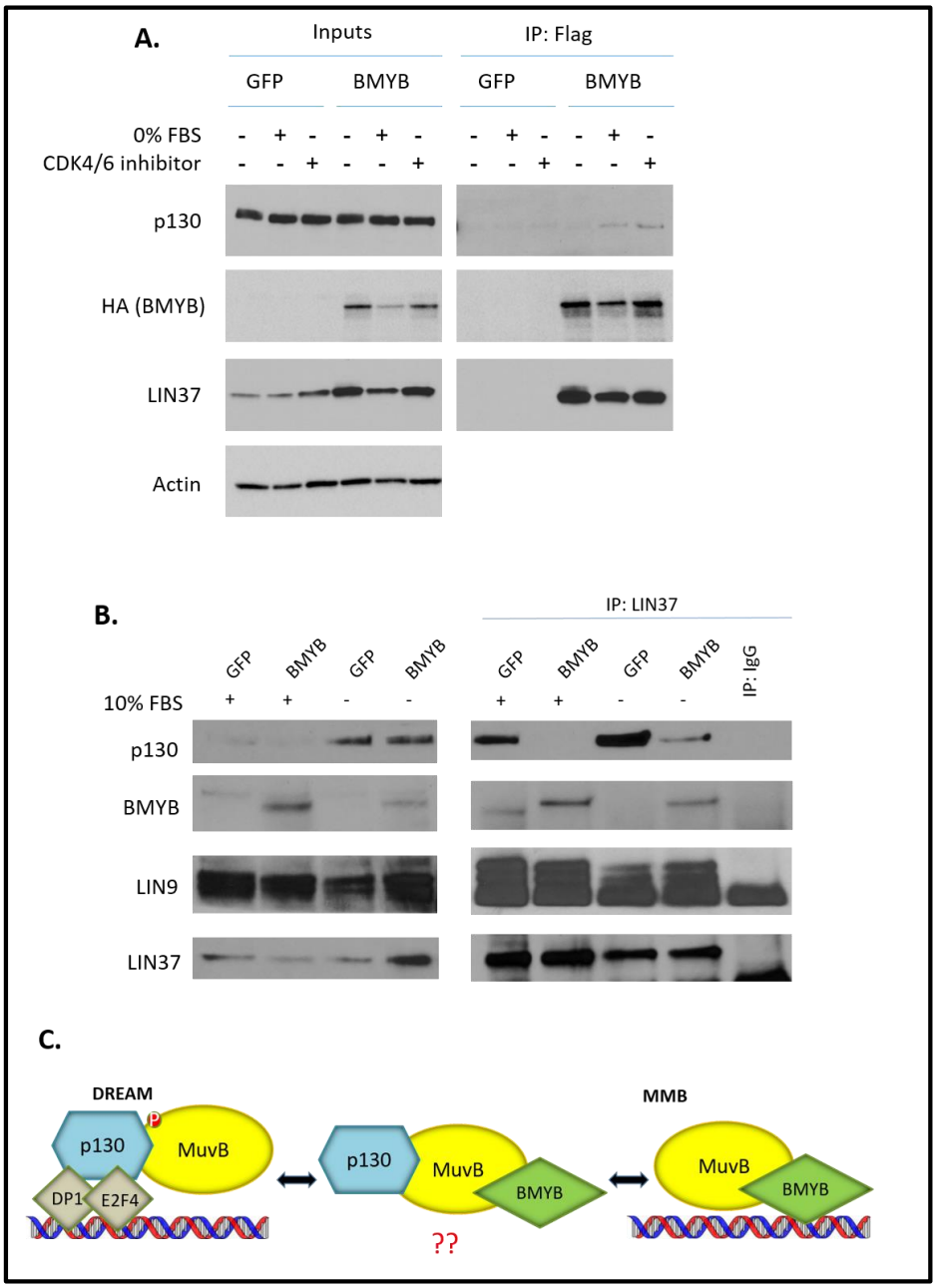

Figure 17. Under certain conditions, p130 and BMYB can simultaneously bind MuvB. (A) BJ-hTERT fibroblasts stably expressing HA-Flag-tagged GFP (control) or BMYB were incubated for 24h in complete medium, medium without FBS, or in medium containing CDK4/6 inhibitor palbociclib. Extracts were immunoprecipitated with anti-Flag antibody, and the indicated proteins were detected by Western blot. (B) Same as in A except cells were incubated for 24 h in complete medium or medium without FBS and extracts were immunoprecipitated with anti-LIN37 antibody. (C) A schematic showing that p130 and BMYB simultaneously bind the MuvB core in a transition state between the DREAM and MMB complexes.

DISCUSSION: CHAPTER 4

4.1. LIN52 directly interacts with p130

In collaboration with Dr. Seth Rubin, we discovered several new structural mechanisms involved in DREAM complex assembly and disassembly. Structural and binding data revealed that LIN52 uses an LxSxExL sequence in combination with phosphorylated S28 to bind the LxCxE cleft within the pocket domain of p130 (Guiley et al, 2015). Given that the LxSxExL sequence in LIN52 is critical for DREAM assembly, mutations in this sequence could alter cellular processes that are normally controlled by the DREAM complex. Similar to the LIN52-S28A mutant, we found that the LIN52-E22A mutant also disrupts DREAM assembly. During G0/G1, the DREAM complex is known to prevent cell cycle entry by repressing a variety of cell cycle dependent genes (Litovchick et al, 2007). Therefore, disrupting DREAM assembly by mutating E22 within the LIN52 LxSxExL sequence could promote escape from quiescence resulting in expression of cell cycle dependent genes.

These findings strongly suggest that LIN52 is key component of the DREAM complex where changes in the expression levels or phosphorylation of this protein could alter DREAM assembly and function. Therefore, it would be interesting in the future to characterize the mechanisms regulating LIN52 protein expression. Given that knockdown of DYRK1A and disruption of its kinase activity result in increased levels of LIN52 protein (L. Litovchick, personal communication), DYRK1A activity may regulate LIN52 protein stability. Furthermore,

the LIN52-S20C mutant can co-precipitate greater amounts of p130 and is expressed at higher levels than wild type LIN52. As a result, LIN52 could be more stable when bound to p130.

4.2. DREAM disassembly by viral oncoproteins

We discovered that LIN52 and the LxCxE domain of the viral oncoproteins bind to the same cleft in p130/p107. Furthermore, the weaker LxSxExL motif in LIN52 enables DREAM disassembly by viral oncoproteins. However, when LIN52 is mutated to mimic the canonical LxCxE motif, the DREAM complex is stabilized in the presence of viral oncoproteins. In addition, we found that the LIN52 S20C mutant reduces the proliferative effects of viral oncoproteins in both MEFs and HeLa cells. Interestingly, in the presence of viral oncoproteins, the expression of wild type LIN52 in MEFs also resulted in growth suppression even though it was unable to rescue DREAM complex assembly. Therefore, growth suppression by wild type LIN52 could be mediated by a different mechanism in MEFs. Given that LIN52 is also part of the MMB complex required for G2/M gene expression, cells over expressing wild type LIN52 could have defects in mitosis resulting in abrogated cellular proliferation. HeLa cells expressing LIN52 S20C had a reduction in colony formation, whereas wild type LIN52 expression did not alter colony formation. Given that a clonogenic assay is another measure of cellular proliferation (Franken et al, 2006), it is possible that an MTT assay is not the best method to monitor proliferation in MEFs. Therefore, in future studies it would be interesting to use other methods such as direct cell counting, BrdU incorporation or Ki-67 staining to measure changes in cellular proliferation.

Previously reported animal models focused on characterizing DREAM loss of function by targeting LIN9 or the p130/p107 pocket domain. However, modifying or removing these proteins in mice causes embryonic or neonatal lethality (Forristal et al, 2014; Reichart et al,

2010). This could be due to LIN9 and p130/p107 having other functions outside of the DREAM complex. Our study shows that the LxSxExL sequence in LIN52 is critical for DREAM assembly where mutating this sequence to mimic the LxCxE motif stabilizes the DREAM complex and reduces cellular proliferation in the presence of viral oncoproteins. Therefore, targeting the LIN52 LxSxExL sequence could be a more direct approach to develop a DREAM complex animal model. For example, to determine the effects of DREAM gain of function on tumorigenesis, we could generate a LIN52 S20C "Super DREAM" mutant mouse and cross it with a mouse tumor model that expresses viral oncoproteins.

4.3. DREAM disassembly by CDK 4/6 phosphorylation

CDK phosphorylation is a well-characterized mechanism for inactivating pocket proteins and inhibiting pocket protein interactions (reviewed in Malumbres & Barbacaid, 2009). In support of this, our study shows that CDK phosphorylation of p130 inactivates the DREAM complex by dissociating pocket proteins from the MuvB core. We found that the binding between the MuvB core and p130 decreases as p130 phosphorylation increases. Furthermore, mutating the conserved CDK sites T401 and T417 to alanine residues enhances growth suppression and stabilizes the DREAM complex. Given that p130 has multiple CDK phosphorylation sites (Hansen et al, 2001), it is possible that additional CDK sites may also contribute to DREAM dissociation by inhibiting LIN52 binding to p130. In addition, for future studies it would be interesting to determine if increased CDK activity promotes MMB formation by excluding p130 from the MuvB core. This could be the mechanism by which CDK activity disrupts the DREAM complex to promote cell cycle progression. Furthermore, CDK inhibitors are currently in clinical trials for different cancers (Chen et al, 2014; DeMichele et al, 2014). Therefore, our findings could be relevant for predicting cancer sensitivity to these drugs.

4.4. BMYB and p130 simultaneously form a complex with MuvB

Previous studies have shown that BMYB and p130 are not found together in complexes purified from mammalian cells, whereas both Myb and Rbf are found together in the *D. melanogaster* dREAM complex (Litovchick et al, 2007; Georlette, 2007; Lewis, 2007). However, our study found that BMYB, p130 and the MuvB core can exist as a complex under conditions in which BMYB is ectopically expressed and p130 is hypophosphorylated. It is possible that this complex was not previously reported because of the coincidental timing of BMYB expression and p130 phosphorylation in the cells used for proteomic analysis. Therefore, our data suggests that the simultaneous binding of BMYB and p130 to the MuvB core is a transition state between the DREAM and MMB complexes (Figure 17C).

High levels of BMYB have been reported in several types of cancer (Thorner et al, 2009; O'Connell et al, 2010; Astbury et al, 2011) and could promote mitotic gene expression by perturbing DREAM assembly. In support of this, we found that overexpression of BMYB reduces DREAM assembly in both cycling and serum deprived cells. This finding is particularly interesting in the case of serum-deprived cells, which is a condition that is normally favorable for DREAM assembly. In future studies, it would be interesting to determine the functional consequences of BMYB overexpression and whether DREAM assembly could be restored by depleting BMYB from cancer cells overexpressing this oncogenic transcription factor.

Understanding DREAM assembly and regulation improves our knowledge of cell cycle exit pathways, which are frequently perturbed in cancer. Our data provides insight into the

mechanisms that negatively regulate DREAM complex assembly and function in cancer, while revealing potential therapeutic targets to halt tumor cell proliferation or dormancy.

CONCLUSION: CHAPTER 5

In summary, this study reports several new mechanisms and biochemical interactions that govern DREAM assembly, disassembly, and function. We found that the MuvB component, LIN52, directly interacts with the pocket domain of p130 using a suboptimal LxSxExL sequence in combination with phosphorylated S28. Furthermore, mutating this sequence to mimic the canonical LxCxE motif found in viral oncoproteins reduces cellular proliferation and stabilizes the DREAM complex in the presence of viral proteins. We addressed how the DREAM complex is disassembled upon cell cycle entry and found that CDK phosphorylation of p130 inactivates the DREAM complex by displacing p130 from the MuvB core. Under certain conditions, we found that BMYB and pl30 simultaneously bind the MuvB core, while overexpression of BMYB disrupts DREAM assembly. Our study provides insight into the molecular architecture of DREAM complex assembly and disassembly, and how these associations are manipulated during cell cycle entry. Further biological studies are needed to test the significance of these interactions on normal cellular function, *in vivo*, and under disease conditions.

LIST OF REFERENCES

1. Aguirre-Ghiso, J. (2007). Models, mechanisms and clinical evidence for cancer dormancy. *Nature Reviews*, 7: 834-846.

2. Aroian, R., Koga, M., Mendel, J., Ohshima, Y., & Sternberg, P. (1990). The let-23 gene necessary for Caenorhabditis elegans vulval induction encodes a tyrosine kinase of the EGF receptor subfamily. *Nature*, 348: 693-699.

3. Astbury, K., McEvoy, L., Brian, H., Spillane, C., Sheils, O., Martin, C., & O'Leary, J. (2011). MYBL2 (B-MYB) in cervical cancer: putative biomarker. *Int J Gynecol Cancer*, 21: 206-212.

4. Beall, E., Manak, J., Zhou, S., Bell, M., Lipsick, J., & Botchan, M. (2002). Role for a Drosophila Myb-containing protein complex in site-specific DNA replication. *Nature*, 420: 833-837.

5. Becker, W., Weber, Y., Wetzel, K., Eirmbter, K., Tejedor, F., & Joost, H. (1998). Sequence characteristics, subcellular localization, and substrate specificity of DYRK-related kinases, a novel family of dual specificity protein kinases. *Journal of Biological Chemistry* , 273: 25893-25902.

6. Beitel, G., Clark, S., & Horvitz, H. (1990). Caenorhabditis elegans ras gene let-60 acts as a switch in the pathway of vulval induction. *Nature*, 348: 503-509.

7. Bertoli, C., Skotheim, J., & de Bruin, R. (2013). Control of cell cycle transcription during G1 and S phases. *Nature*, 14: 518-528.

8. Blais, A., & Dynlacht, B. (2004). Hitting their targets: an emerging picture of E2F and cell cycle control. *Current Opinion in Genetics & Development*, 14: 527-532.

9. Canhoto, A., Chestukhin, A., Litovchick, L., & DeCaprio, J. A. (2000). Phosphorylation of the retinoblastoma-related protein p130 in growth arrested cells . *Oncogene*, 44: 5116-5122.

10. Chen, E., Hotte, S., Hirte, H., Siu, L., Lyons, J., Squires, M., . . . Seymour, L. (2014). A Phase I study of cyclin-dependent kinase inhibitor, AT7519, in patients with advanced cancer: NCIC Clinical Trials Group IND 177. *Br J Cancer*, 111: 2262-2267.

11. Chen, J., Lin, J., Tsai, F., & Meyer, T. (2013). Dosage of DYRK1A shifts cells within a p21-cyclin D1 signaling map to control the decision to enter the cell cycle. *Molecular Cell*, 52: 87-100.

12. Chen, X., Müller, G., Quaas, M., Fischer, M., Han, N., Stutchbury, B., . . . Engeland, K. (2013). The forkhead transcription factor FOXM1 controls cell cycle-dependent gene expression through an atypical chromatin binding mechanism. *Mol. Cell. Biol.*, 33: 227-236.

13. Clarke, M., Dumon, S., Ward, C., Jäger, R., Freeman, S., Dawood, B., . . . García, P. (2013). MYBL2 haploinsufficiency increases susceptibilty to age-related haematopoietic neoplasia. *Leukemia*, 27: 661-670.

14. Classon, M., & Harlow, E. (2002). The retinoblastoma tumor suppressor in development and cancer. *Nature Reviews*, 2: 910-917.

15. Cobrinik, D. (2005). Pocket proteins and cell cycle control. *Oncogene*, 24: 2796–2809.

16. Dannenberg, I., Schuijff, L., Dekker, M., van der Valk, M., & Riele, H. (2004). Tissue specific tumor suppressor activity of retinoblastoma gene homologues p107 and p130. *Genes & Development*, 18: 2952-2962.

17. DeCaprio, J. (2014). Human papillomavirus type 16 E7 perturbs DREAM to promote cellular proliferation and mitotic gene expression. *Oncogene*, 33: 4036-4038.

18. DeCaprio, J. A. (2009). How the Rb tumor supressor structure and function was revealed by the study of Adenovirus and SV40. *Virology*, 384: 274-284.

19. DeGregori, J. (2002). The genetics of the E2F family of transcription factors: shared functions and unique roles. *Biochim. Bio. Acta*, 1602: 131-150.

20. DeMichele, A., Clark, A., Tan, K., Heitjan, D., Gramlich, K., Gallagher, M., . . . O'Dwyer, P. (2015). CDK4/6 Inhibitor Palbociclib(PD0332991) in Rbþ Advanced Breast Cancer: PhaseII Activity, Safety, and Predictive Biomarker Assessment . *Clin. Cancer Res.* , 995-1001.

21. Dick, F. A., & Rubin, S. M. (2013). Molecular mechanisms underlying RB protein function. *Nature Reviews*, 14: 297-306.

22. Down, C., Millour, J., Lam, E., & Watson, R. (2012). Binding of FoxM1 to G2/M gene promoters is dependent upon B-Myb. *Biochim. Biophus. Acta*, 1819: 855-862.

23. Fay, D., & Han, M. (2000). The synthetic multivulval genes of C. elegans: functional redundancy, Ras antagonism, and cell fate determination. *Genesis*, 26: 279-284.

24. Felsani, A., Mileo, A. M., & Paggi, M. G. (2006). Retinoblastoma family proteins as key targets of small DNA virus oncoproteins. *Oncogene*, 25: 5277-5285.

25. Ferguson, E., & Horvitz, H. (1989). The multivulva phenotype of certain Caenorhabditis elegans mutants results from defects in two functionally redundant pathways. *Genetics*, 123: 109-121.

26. Florens, L., & Wasburn, M. (2006). Proteomic analysis by multidimensional protein identification technology . *Methods Mol Biol*, 328: 159-175.

27. Forristal, C., Henley, S. A., MacDonald, J. I., Bush, J. R., Ort, C., Passos, D. T., . . . al, e. (2014). Loss of mammalian DREAM complex deregulates chondrocyte proliferation . *Molecular and Cellular Biology* , 2221-2234.

28. Franken, N., Rodermond, H., Stap, J., Haveman, J., & van Bree, C. (2006). Clonogenic assay of cells in vitro. *Nature Protoc.*, 1:2315-2319.

29. Georlette, D., Ahn, S., MacAlpine, D., Cheung, E., Lewis, P., Beall, E., . . . Botchan, M. (2007). Genomic profiling and expression studies reveal both positive and negative activities for the Drosophila Myb MuvB/dREAM complex in proliferating cells. *Genes & Development*, 21: 2880-2896.

30. Giacinti, C., & Giordano, A. (2006). RB and cell cycle progression. *Oncogene*, 25: 5220-5227.

31. Guiley, K. Z., Liban, T. J., Felthousen, J. G., Ramanan, P., Litovchick, L., & Rubin, S. M. (2015). Structural mechanisms of DREAM complex assembly and regulation. *Genes & Development*, 29: 1-15.

32. Han, M., & Sternberg, P. (1990). let-60, a gene that specifies cell fates during C. elegans vulval induction, encodes a ras protein. *Cell*, 63: 921-931.

33. Hansen, K., Farkas, T., Lukas, J., Holm, K., Rönnstrand, L., & Bartek, J. (2001). Phosphorylation-dependent and -independent functions of p130 cooperate to evoke a sustained G1 block. *EBMO J*, 20:422-432.

34. Helt, A., & Galloway, D. (2003). Mechanisms by which DNA tumor virus oncoproteins target the Rb family of pocket proteins. *Carcinogenesis*, 24: 159-169.

35. Himpel, S., Panzer, P., Eirmbter, K., Czajkowska, H., Sayed, M., Packman, L., . . . Becker, W. (2001). Identification of the autophosphorylation sites and characterization of their effects in the protein kinase DYRK1A. *Biochem. J*, 359: 497-505.

36. Hurford, R., Cobrinik, D., Lee, M., & Dyson, N. (1997). pRB and p107/p130 are required for the regulated expression of different sets of E2F responsive genes. *Genes & Development*, 11: 1447-1463.

37. Javier, R., & Butel, J. (2008). The history of tumor virology. *Cancer Res.*, 68: 7693-7706.

38. Korenjak, M., Taylor-Harding, B., Binné, U., Satterlee, J., Stevaux, O., Aasland, R., . . . Brehm, A. (2004). Native E2F/RBF complexes contain Myb-interacting proteins and repress transcription of developmentally controlled E2F target genes. *Cell*, 119: 181-193.

39. Korver, W., Roose, J., Wilson, A., & Clevers, H. (1997). The winged-helix transcription factor Trident is expressed in actively dividing lymphocytes. *Immunobiology*, 198: 157-161.

40. Lammens, T., Li, J., Leone, G., & De Veylder, L. (2009). Atypical E2Fs: new players in the E2F transcription factor family . *Cell* , 111-118.

41. Laoukili, J., Kooistra, M., Brás, A., Kauw, J., Kerkhoven, R., Morrison, A., . . . Medema, R. (2005). FoxM1 is required for execution of the mitotic programme and chromosome stability. *Nature Cell Biol.*, 7: 126-136.

42. Lewis, P., Beall, E., Fleischer, T., Georlette, D., Link, A., & Botchan, M. (2004). Identification of a Drosophila Myb-E2F2/RBF transcriptional repressor complex . *Genes & Development* , 18: 2929-2940.

43. Litovchick, L., Florens, L. A., Swanson, S. K., Washburn, M. P., & DeCaprio, J. A. (2011). DYRK1A protein kinase promotes quiescence and senescence through DREAM complex assembly. *Genes & Development*, 25: 801-813.

44. Litovchick, L., Sadasivam, S., Florens, L., Zhu, X., Swanson, S. K., Velmurugan, S., . . . DeCaprio, J. A. (2007). Evolutionary conserved multisubunit RBL2/p130 and E2F4 protein complex represses human cell cycle-dependent genes in quiescence. *Molecular Cell*, 26: 539-551.

45. Malumbres, M., & Barbacid, M. (2009). Cell cycle, CDKs and cancer: a changing paradigm. *Nature Reviews*, 9: 153-166.

46. Malumbres, M., & Barcacid, M. (2001). To cycle or not to cycle: a critical decision in cancer. *Nature Reviews*, 1: 222-231.

47. Moran, E. (1993). DNA tumor virus transforming proteins and the cell cycle. *Current Opinions in Genetics & Development*, 3: 63-70.

48. Mullier, F., Daliphard, S., Garand, R., Dekeyser, M., Cornet, Y., Luquet, I., . . . Chatelain, B. (2012). Morphology, cytogenetics, and survival in myelodysplasia with del(20q) or ider(20q) a multicenter study. *Ann. Hematol.*, 91: 203-213.

49. O'Connell, M., Lavery, I., Yothers, G., Paik, S., Clark-Langone, K., Lopatin, M., . . . Wolmark, N. (2010). Relationship between tumor gene expression and recurrance in four independent studies of patients with stage II/III colon cancer treated with surgery alone or surgery plus adjuvant fluorouracil plus leurcovorin. *J. Clin. Oncol.*, 28: 3937-3944.

50. Osterloh, L., von Eyss, B., Schmit, F., Rein, L., Hubner, D., Samans, B., . . . Gaubatz, S. (2007). The human synMuv-like protein LIN-9 is required for transcription of G2/M genes and for entry into mitosis. *EMBO J* , 26: 144-157.

51. Pilkinton, M., Sandoval, R., & Colamonici, O. (2007). Mammalian Mip/LIN-9 interacts with either the p107, p130/E2F4 repressor complex or B-Myb in a cell cycle-phase-dependent context distinct from the Drosophila dDREAM complex. *Oncogene*, 26: 7535-7543.

52. Poulin, D., & DeCaprio, J. A. (2006). Is there a role for SV40 in human cancer? *Journal of Clinical Oncology*, 24: 4356-4364.

53. Rashid, N. N., Yusof, R., & Watson, R. J. (2011). Disruption of repressive p130-DREAM complexes by human papillomavirus 16 E6/E7 oncoproteins is required for cell-cycle progression in cervical cancer cells. *Journal of General Virology*, 92: 2620-2627.

54. Reichart, N., Wurster, S., Ulrich, T., Schmitt, K., Hauser, S., Probst, L., . . . Gaubatz, S. (2010). Lin9, a subunit of the mammalian DREAM complex, is essential for embryonic development, for survival of adult mice, and for tumor suppression. *Molecular and Cellular Biology* , 2896-2908.

55. Sadasivam, S., & DeCaprio, J. (2013). The DREAM complex: master coordinator of cell cycle-dependent gene expression. *Nature Reviews*, 1-9.

56. Sadasivam, S., Duan, S., & DeCaprio, J. A. (2012). The MuvB complex sequentially recruits B-Myb and FoxM1 to promote mitotic gene expression. *Genes & Development*, 26: 474-489.

57. Schafer, K. A. (1998). The cell cycle: a review. *Vet Pathol*, 35: 461-478.

58. Scholzen, T., & Gerdes, J. (2000). The Ki-67 protein: from the known and the unknown. *J Cell Physiol.*, 182:311-322.

59. Shepard, J., Amatruda, J., Stern, H., Subramanian, A., Finkelstein, D., Ziai, J., . . . Zon, L. (2005). A zebrafish bmyb mutation causes genome instability and increased cancer susceptibility. *Proc. Natl Acad. Sci. USA*, 102: 13194-13199.

60. Soppa, U., Schumacher, J. F., Pasqualon, T., Tejedor, F., & Becker, W. (2014). The Down syndrome-related protein kinase DYRK1A phosphorylates p27(Kip1) and Cyclin D1 and induces cell cycle exit and neuronal differentiation. *Cell Cycle*, 13: 2084-2100.

61. Thorner, A., Hoadley, K., Parker, J., Winkel, S., Millikan, R., & Perou, C. (2009). In vitro and in vivo analysis of B-Myb in basal-like breast cancer. *Oncogene,* 28: 742-751.

62. Zhu, W., Giangrande, P., & Nevins, J. (2004). E2Fs link the control of G1/S and G2/M transcription. *EMBO J,* 23: 4615-4626.